POLITECNICO
MILANO 1863

SCUOLA DI INGEGNERIA INDUSTRIALE
E DELL'INFORMAZIONE

Role of f-hole design in stress distribution and radiation of the violin

Tesi di Laurea Magistrale in
Music and Acoustic Engineering

Author: **Lorenzo Previati**

Student ID: 222058
Advisor: Prof. Fabio Antonacci
Co-advisors: Juan Sebastian Gonzalez Briones
Academic Year: 2025-26

Abstract

This thesis addresses the parametric analysis of the influence of f-holes geometry on the structural and acoustic performance of the violin soundboard. Although the shape of the f-holes is crucial for sound emission, the quantitative interaction between their geometry and the board's mechanics is not fully characterized in the literature Using the Finite Element Method (FEM) with a model incorporating the orthotropic properties of wood, the study examines a series of design configurations, varying key geometric parameters such as area and perimeter. The analysis, performed with a coupled FEM-BEM method, focuses on the variation of eigenfrequencies and the acoustic radiation efficiency, quantified by the far-field Sound Pressure Level (SPL). Through statistical analysis, it was possible to quantify the correlation between vibrational and acoustic variability. The results provide a quantitative mapping that correlates geometric changes in the f-holes with eigenfrequency shift and stress distribution, supporting design decisions aimed at optimally balancing structural stiffness and acoustic response.

Keywords: Violin, F-holes, FEM-BEM, Parametric analysis, Vibrational modes, Stress, SPL.

Abstract in lingua italiana

Questa tesi affronta l'analisi parametrica dell'influenza della geometria degli f-holes sulle prestazioni strutturali e acustiche della tavola armonica del violino. Sebbene la forma delle effe sia cruciale per l'emissione sonora, l'interazione quantitativa tra la loro geometria e la meccanica della tavola non è pienamente caratterizzata in letteratura. Utilizzando il Metodo degli Elementi Finiti (FEM) con un modello che incorpora le proprietà ortotrope del legno, lo studio esamina una serie di configurazioni di design, variando i parametri geometrici principali come area e perimetro. L'analisi, svolta con un metodo FEM-BEM accoppiato, si concentra sulla variazione delle autofrequenze e sull'efficienza di irraggiamento acustico, quantificata tramite il Livello di Pressione Sonora (SPL) in campo lontano. Attraverso un'analisi statistica, è stato possibile quantificare la correlazione tra variabilità vibrazionale ed acustica. I risultati forniscono una mappatura quantitativa che correla le modifiche geometriche delle effe con lo shift delle autofrequenze e la distribuzione dello stress, supportando decisioni di design mirate al bilanciamento ottimale tra rigidezza strutturale e risposta acustica.

Parole chiave: Violino, F-holes, FEM-BEM, Analisi parametrica, Modalità vibrazionali, Stress, SPL.

Contents

1 | Introduction

The violin, which reached its peak during the Cremonese period between the 17th and 18th centuries with master luthiers such as Nicola Amati (1596–1684) and later Antonio Stradivari (1644–1737) and Giuseppe Guarnieri del Gesù (1698–1744), is one of the most sophisticated and important musical instruments in the music world. However, the assumption of the tonal superiority of antique violins over modern ones was challenged by double-blind studies conducted in 2014 [1]. These tests demonstrated that soloists are not always able to distinguish historical instruments from new ones, often preferring the latter for their dynamic qualities and ease of response, confirming that acoustic quality remains a highly subjective attribute and difficult to define unequivocally [2]. In this context, related studies from 2015 suggest that understanding the mechanisms by which musicians evaluate an instrument is a fundamental step in identifying physical quality parameters [3]. Given the difficulty of establishing a perceptual consensus, the mechanical study of individual structural components becomes a priority. This research aims to define objective physical and geometric parameters capable of mapping the real influence of design on the instrument's performance. Despite centuries of scientific study, the relationship between geometry and acoustic performance remains a topic of active research. Among the components that make up this instrument, the f-holes play a critical role in determining the vibrational and acoustical properties. Some numerical studies have attempted, through extreme geometric modifications that go beyond traditional design standards, to show the correlation between the size of the f-holes and the mechanical response of the entire instrument [4]. The f-holes thus represent, in addition to a factor of physical variability, an element that characterizes the design and historical identity of a violin; for this reason, the great master luthiers have paid particular attention to their shape, proportion, and position. It is in this context that this study offers its contribution: the systematic and parametric analysis of f-holes aims not to define a subjective quality, but to provide an objective mechanical and acoustic characterization, which is important for supporting future directions in instrument design and production.

1.1. Evolution and role of f-holes

Modern f-holes are the result of a gradual evolution throughout history. This evolution saw f-holes change their shape from the circular harmonic holes of 10th-century viols, through semicircular C-shaped openings, to reach their current configuration. Compared to circular holes, f-holes produce, for the same area, a higher radiated power of approximately 60%, demonstrating a clear improvement in acoustic performance. This substantial increase is due to the fact that acoustic conductance is proportional to the perimeter, rather than the area, of the holes, as airflow is more concentrated along the edges of the holes than inside them [5].

Figure 1.1: Holes shape historical evolution Source: [5]

Recent numerical model-based screening studies have confirmed that geometric design choices, including the configuration of the f-holes, have a predominant impact on instrument dynamics compared to the intrinsic variability of the wood material [6]. The main role of the f-hole is to increase the efficiency of low-frequency radiation, thanks to the vibration of the internal air volume and in proximity to the opening that reshapes the boundary conditions [7]. In particular, it has already been studied, both through analytical models and through computational simulation models, that this mechanism occurs mainly in correspondence with the A0 mode, called Helmholtz resonance [4, 8, 9]. Recent studies, using simulations with coupling between the Finite Element Method (FEM) and the Boundary Element Method (BEM), have revealed that an increase in the size of the f-holes increases the sound power not only for low frequencies, but also affects the radiation level for higher frequencies. Having explained this, it is important to underline that already in the Cremonese period a tendency to lengthen the f-holes by about 30% had emerged, a modification associated with increased radiated power. This suggests the presence of an implicit, experience-based understanding of the instrument's acoustic behavior [5].

1.2. The great master luthiers

Great luthiers developed different approaches to f-hole design. Nicola Amati, one of the most prominent figures of the Cremonese luthier, developed particularly refined f-holes, but with shorter openings, resulting in less radiated power, which was preferable for performances in small venues [10]. Giuseppe Guarnieri del Gesù, influenced by the Brescia school luthier Giovanni Paolo Maggini (1580-1630), developed more elongated and asymmetrical f-holes [11]. In contrast to the Cremonese tradition, the Tyrolean violin maker Jacob Stainer (c. 1618–1683) developed a different f-hole geometry, characterized by shorter, vertical openings with a pronounced curvature of the soundboard [12]. This design influenced European violin making for decades, offering a distinct structural rigidity and acoustic response compared to later Stradivari models. Antonio Stradivari was the Cremonese luthier who most significantly changed the construction approach by focusing his attention on proportions modeled through the golden section, in turn evolving the position and type of openings used in his instruments, more slender and with deeper niches [13]. Stradivari explored alternative solutions for soundboard design, developing prototypes with unconventional shapes and acoustic properties. One example is the 1726 'cornerless' violin, now known as the 'Chanot-Chardon-Braga' [14], which inspired the model in this study. Its guitar-like profile represents an important historical precedent for cornerless instruments. This design was later revived and refined in the 19th century by François Chanot for his experimental violins. The evolution of f-holes was therefore the result of an iterative process, which led to a substantial redesign of the openings, including shape, size, proportions and orientation.

1.3. "Cornerless" violins and structural variations

The "cornerless" violin is one of the most interesting examples of alternative designs that offer the possibility of more easily studying how structural variations influence stress distribution and acoustic radiation. The first model with this particular design was built by Antonio Stradivari, only to be taken up by later scholars such as Francois Chanot (1788-1825), who designed a "cornerless" violin with simplified f-holes aligned along the edge [15]. This type of configuration has not gained widespread adoption among musicians and luthiers, but has become important for various scientific studies. The effectiveness of this model lies in the fact that the absence of corners modifies the connection stiffness between the structural blocks, altering their stress flow. This configuration, therefore, allows for the geometry to be simplified in order to isolate the contribution of the f-hole design to the vibrational and acoustic behavior of the instrument. Recent studies have

shown that the dynamic behavior of the violin is more dependent on geometric parameters such as the shape of the f-holes and the thickness and curvature of the top plate, than on the elastic properties of the material used [16]. For these reasons, "cornerless" violins are excellent for simplifying the geometry and focusing on the impact of the f-holes on the overall behavior of the model.

1.4. Computational modeling of violin acoustics

Numerical modeling of stringed instruments has undergone constant evolution, moving from the study of individual components to the analysis of complex vibro-acoustic systems. As highlighted in a recent systematic review, string instruments are considered complex mechanical vibrating systems where the sound production is governed by the interaction between the structure and the surrounding fluid [17]. In this context, the FEM method has established itself as the standard tool for simulating the behavior of the soundboard and the resonance chamber [17, 18]. Computational mathematical methods have revolutionized the study of violin physics, offering the possibility of analyzing acoustic-structural coupling phenomena with a spatial resolution and parametric flexibility difficult to achieve solely with experimental techniques [19]. While FEM is ideal for internal structural dynamics, BEM has emerged as a superior tool for calculating sound radiation. The main advantage of BEM lies in its ability to satisfy the radiation condition at infinity without requiring a mesh for the entire external air domain, effectively reducing the problem's dimensionality [20]. This coupled approach allows for both uncoupled analysis, where surface velocities serve as boundary conditions, and fully coupled fluid-structure interaction (FSI) analysis, where the air mass loading effect is explicitly considered. However, contemporary research is moving towards data-driven paradigms to overcome the high computational costs of traditional simulations. It has been demonstrated that Neural Networks can effectively learn the complex relationship between geometric parameters and vibrational response, allowing the prediction of the eigenfrequencies of a soundboard significantly faster than conventional FEM [21]. A significant advance in this field is the FRF2Params technique, which uses NNs to solve the inverse problem of wood characterization starting from a single Frequency Response Function, implicitly acquiring information about mode shapes through the behavior of peak amplitudes [22]. Regarding sound radiation, recent research has shown that neural networks can be trained on FEM datasets to predict not only vibrational properties but also far-field acoustic radiation (SPL). This approach has demonstrated remarkable computational efficiency, reaching speeds up to 6000 times compared to traditional solvers, allowing real-time evaluation of design variations [23]. Despite the efficiency of structural

models, the state of the art highlights that simulations conducted solely on the structure do not fully capture the physical complexity of the instrument. The integration of air in the simulations is crucial, as it produces an added mass effect that lowers the natural frequencies of the body modes and alters the radiative response compared to vacuum models [24]. Experimental studies conducted using acoustic holography have confirmed that the contribution of f-holes to far-field radiation is significant across the entire audible spectrum and tightly coupled to the motion of the structure [25]. The use of coupled approaches such as FEM-BEM is therefore essential to obtain reliable predictive models that correctly consider fluid-structure interaction and radiation efficiency [26]. In this context, while parametric studies have explored the impact of the positioning of the f-holes on the frequency of the "Bridge Hill" [27], or analyzed the effect of the size scale of the sound holes [5], a gap remains in the literature regarding the systematic characterization of the purely geometric influence of the different historical profiles. This thesis addresses this gap, using the coupled FEM-BEM methodology to investigate how variations in the shape, area, and perimeter of the f-holes, given the same position and structural conditions, affect the stress distribution and acoustic radiation [28]. The adoption of a "cornerless" model also allows us to isolate the geometric contribution of the openings, providing an objective basis that integrates traditional construction knowledge [29] with the rigor of advanced numerical modeling.

1.5. Research context and contribution

Recent studies have employed the coupled FEM-BEM method to investigate how the size of f-holes affects the modal and acoustic responses, but have primarily focused on the parametric scale of a single design, altering its dimensions while keeping the aspect ratio fixed. By analyzing six different scales of the same design (70% -110% of the original size), it was possible to understand the effects of the opening size on the response behavior of the violin [4]. Another important study conducted by MIT in 2015 analyzed the role of f-holes in radiated sound power, demonstrating a 60% increase as a result of the evolution of the historical design. The study analyzed historical violins to determine trends in the elongation of the openings that developed over time, but did not compare specific hole geometries under fixed structural conditions [5]. Despite advances in numerical acoustics, a numerical model that incorporates all components of the complete instrument geometry, fluid-structure interaction, and interaction with the surrounding air remains a significant computational challenge and has not yet been fully simulated [17]. Due to these high computational demands, many studies remain limited to single components or simplified models. It is in this context that this thesis fits in, to study the influence of a design

variation of f-holes on the vibrational and acoustic response of the instrument through coupled mathematical simulation methods.

In this study, a coupled FEM-BEM investigation was conducted comparing five different historically relevant f-hole designs (Amati, Stradivari, Maggini, Guarnieri, Stainer) applied to a cornerless violin model. The study methodology used is modeled on a 2022 study, conducted on guitars, which explored the use of wooden mechanical metamaterials to regulate the mechanical properties of soundboards [28]. The FEM simulation, carried out on the top plate, allows the distribution of stress and deformation to be studied in relation to the f-hole design applied. The relationship between the maximum deformation on the centre line of the top plate and the area and perimeter parameters of the different opening designs were calculated in order to find the best linear correlation. The results showed that the vibrational response, like the already demonstrated acoustic response [10], is more dependent on the perimeter of the opening than on the area. A coupled FEM-BEM simulation was applied to the entire sound box of the violin to study the relationship between variation in mechanical and acoustic response. The vibration modes characterized by the highest standard deviation value among the various f-hole designs, and following acoustic simulation, the points with the highest Sound Pressure Level (SPL) value were identified. Statistical correlation analysis identified the presence of "mode switching", a phenomenon whereby the frequency approximation of two eigenmodes causes a mutual exchange of characteristics between them [30]. The MAC matrices were calculated, showing the relationships between models with different f-holes. The results of this statistical investigation confirm that 22% of modes with high structural variability are associated with high acoustic variability and that 31.7% of modes with high acoustic variability are associated with high structural variability. The following chapters outline the methods and parameters employed in the simulation, present the results of the analysis conducted, provide a statistical evaluation of the results, and discuss the implications for understanding violin acoustics.

2 | FEM Analysis

FEM was employed using COMSOL in order to investigate the structural response of a cornerless violin top plate as a function of different types of f-hole design. The target was to compare model and static responses for five historical f-holes (Amati, Guarnieri, Maggini, Stainer, and Stradivari) evaluating vibrational behavior and deformation under load. The study analyzes the soundboard to determine the influence of the geometry of the f-holes on the instrument's structural and acoustic response. This approach is based on integrating three-dimensional models, derived from CAD modeling or 3D scanning, with the FEM. As demonstrated, the use of parametric numerical modeling is superior to traditional techniques, as it allows for the isolation and control of each geometric variable with extremely high precision [31]. This virtual manipulation capability allows for the mapping of variations in natural frequencies and sound radiation as a function of the design. The shared goal is the evolution of violin making towards a discipline based on objective data, capable of analytically predicting the impact of each construction choice on the final mechanical and acoustic response.

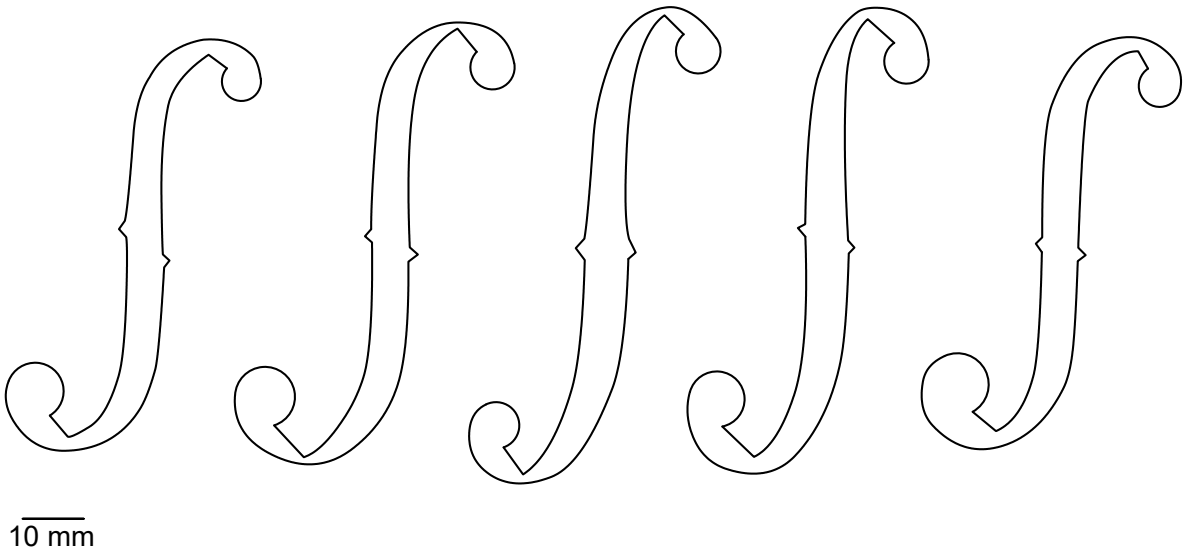

Figure 2.1: f-hole designs: (1) Nicola Amati; (2) Antonio Stradivari; (3) Giovanni Paolo Maggini; (4) Guarnieri del Gesù; (5) Jacob Stainer.

2.1. Geometry and Material

The model studied is that of a cornerless violin, which, unlike traditional violins, has no side corners. In this way, the body curves flow more continuously. The result is a more modern shape with a more minimalist design.

Figure 2.2: Cornerless violin by François Chanot (c. 1820-1823) Source: [32]

The three-dimensional geometry of the soundboard plays an important role in the vibroacoustic response of stringed instruments. Studies on stringed instruments, such as archtop guitars, have demonstrated how the thickness distribution and curvature of the soundboard significantly influence the natural modes of vibration [33]. Similarly, this work analyzes the effect of five soundhole sequences on a violin, keeping the archtop geometry of the soundboard constant. A cornerless violin top plate was modeled in Fusion 360 to minimize geometric variability that is not related to the f-holes. The outline of the top plate is based on a standard full-size violin, and the typical arching is defined by lofted cross-sectional curves.

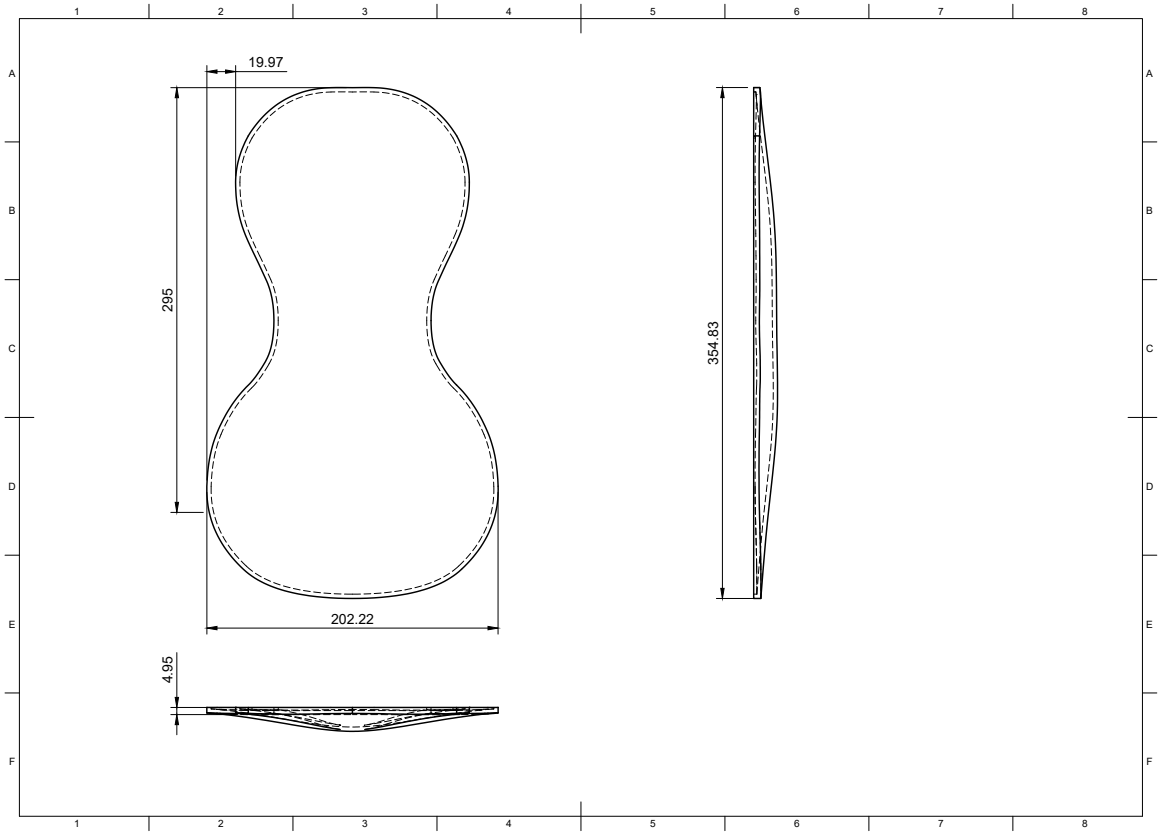

Figure 2.3: Cornerless violin top plate model.

Spruce wood was selected as the material due to its relevance in the application in the acoustic field. The top plate was modeled using orthotropic linear elasticity, which allows different stiffness and deformation along the three axes:

- Longitudinal (L): along the grain direction (maximum stiffness)
- Radial (R): from the center of the tree outward (moderate stiffness)
- Tangential (T): tangential to growth rings (minimum stiffness)

Adopting an isotropic material model would assume uniform behavior in all directions, which is inadequate for wood-based materials. An orthotropic formulation is essential to accurately capture vibrational modes and stress distribution. Wood exhibits orthotropy due to its cellular structure; indeed, mechanical properties such as Young's modulus can vary by more than an order of magnitude between the longitudinal and transverse directions [34]. The elastic behavior is described in three independent constants associated with each direction: Young's Modulus (E_{L}, E_{R}, E_{T}), Shear Modulus (G_{LR}, G_{RT}, G_{LT}) and Poisson's Ratios (ν_{LR}, ν_{RT}, ν_{LT}). These material constants are representative of the spruce used in violin construction and are consistent with measurements made on historic Cremonese instruments, ensuring that the simulation reflects realistic mechanical behavior [4, 23, 35].

Therefore, modeling the top plate as orthotropic is essential to realistically assess how changes in f-hole geometry affect both structural and vibrational behavior, aligning the simulation with the physical properties of real violins. The accuracy of this approach is confirmed by 2019 studies, which validated the use of FEM models based on orthotropic properties to correctly recover the natural frequencies and mode shapes consistent with real violins [36]. This modeling is essential to correctly capture the main resonances of the free plates, whose dynamics are significantly governed by Young's moduli, particularly along the EL fiber direction, and by the material density.

The values used in this study are:

Density [kg/m^3]	Young's Modulus [MPa]			Shear Modulus [MPa]			Poisson's Ration		
ρ	E_{L}	E_{R}	E_{T}	G_{LR}	G_{RT}	G_{LT}	ν_{LR}	ν_{RT}	ν_{LT}
402	12000	925	737	695	217	653	0.38	0.51	0.50

Table 2.1: Material constants. In the subscripts, L refers to the longitudinal component, T refers to the tangential component, and R refers to the radial component. Source: [4]

After negative extrusion of the profiles for the 5 types of f-holes, the resulting geometries were exported in STEP format and imported into COMSOL Multiphysics.

2.2. Eigenfrequencies study

Modal analysis was performed using the FEM to investigate the vibrational behavior of the violin top plate for different f-hole designs. The target of this simulation was to compute the eigenfrequencies (natural frequencies) and the corresponding vibrational mode shapes of the top plate, fundamental to understanding its dynamic acoustic response. For this

type of study, no limits have been set on the top plate boundaries, so it is completely free to vibrate.

The governing equation used in COMSOL for eigenfrequencies analysis is derived from the linear equation in the absence of damping and external loads:

$$-\omega^2 \rho \mathbf{u} = \nabla \cdot \boldsymbol{\sigma}(\mathbf{u})$$

where:

- ω is the angular frequency (rad/s),
- ρ is the material density,
- $\mathbf{u}$ is the displacement field,
- $\boldsymbol{\sigma}(\mathbf{u})$ is the stress tensor, related to strain via the constitutive relation for orthotropic materials.
- $\nabla \cdot \boldsymbol{\sigma}(\mathbf{u})$ it is the divergence of the stress tensor and describes the distribution of internal forces per unit volume, i.e., the elastic forces that bring the body back into equilibrium.

COMSOL enters the relationship between the stress tensor and the strain tensor for a linear orthotropic material. It then rewrites the equation in a weak variational form, which is required in FEM analysis:

$$\int_\Omega \delta \mathbf{u}^T \left(-\omega^2 \rho \mathbf{u} - \nabla \cdot \boldsymbol{\sigma}\right) \, d\Omega = 0$$

At this point, after integrating by parts and substituting the constitutive law, the eigenvalue system is obtained. For domain discretization, it was necessary to set up an extra fine tetrahedral mesh to the domain. The smaller the mesh size, the more accurate the result, but it comes with a higher computational cost.

COMSOL then constructs the matrices:

$$\mathbf{K}\mathbf{u} = \lambda \, \mathbf{M}\mathbf{u}$$

where:

- $\mathbf{K}$ is the stiffness matrix (depends on geometry, material, and boundary conditions),
- $\mathbf{M}$ is the mass matrix (depends on density ρ and the mesh),

- $\lambda = \omega^2$ is the eigenvalue,
- $\mathbf{u}$ is the eigenvector, representing the modal shape.

The last step is the numerical resolution of the system to obtain:

- ω_i: the natural angular frequencies (eigenfrequencies : $f_i = \frac{\omega_i}{2\pi}$),
- $\mathbf{u}_i$: the corresponding vibration mode shapes (eigenmodes).

This eigenvalue formulation is standard in structural dynamics and has been successfully applied to the modal analysis of violins and other stringed instruments using FEM since 1980 with various industrial software [37] The analysis was repeated for each f-hole design, and the first 12 modes were extracted and plotted.

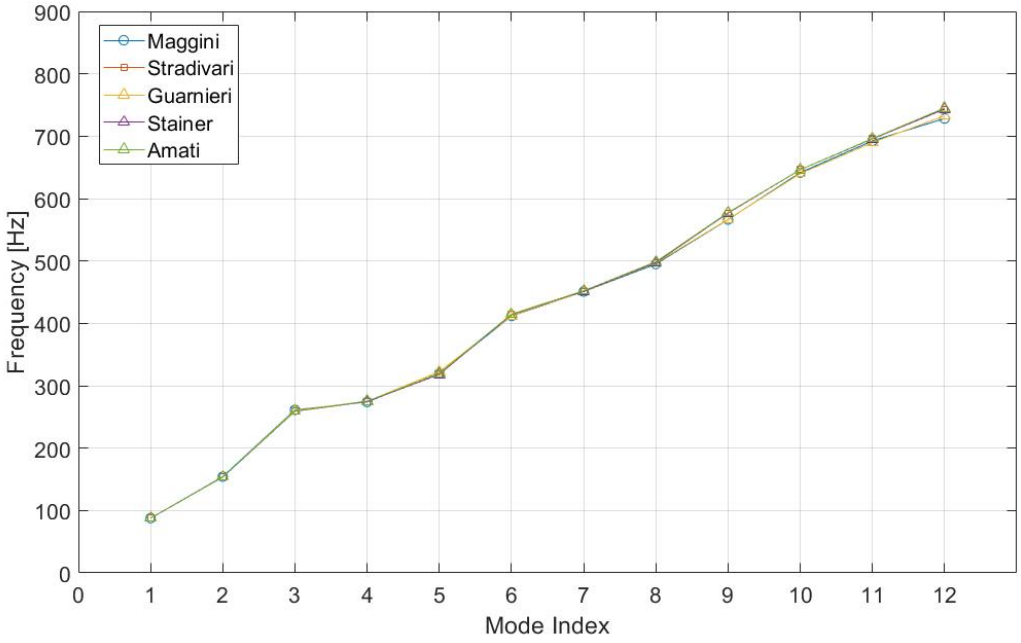

Figure 2.4: First 12 vibrational modes - f-hole designs comparison plot.

From observation of the plot, it can be concluded that below 1000 Hz, there is no significant variation in vibration modes in relation to the type of f-hole design. This implies that the effect of the f-hole shape on the overall vibrational behavior of the top plate is not that significant.However, it is important to note that these free vibration modes describe only the structural response of the system. As already demonstrated, the influence of the enclosed air significantly modifies the natural frequencies compared to vacuum conditions while maintaining the mode shapes virtually unchanged. This fundamental interaction highlights the need to evolve the analysis towards coupled FEM-BEM models, capable

of capturing the global vibroacoustic behavior and overcoming the intrinsic limitations of purely structural simulations [38].

2.3. Stress and Displacement study

To complement the eigenfrequency study, a static structural analysis was conducted in order to evaluate how different f-hole designs influence the stress distribution and the displacement field of the violin top plate. This analysis was conducted using COMSOL Multiphysics under the Solid Mechanics module, with the top plate boundaries fixed and a vertical force of -117 N applied in the bridge region, which approximates the downward pressure exerted by the tensioned strings. Applying a static load in the bridge region is critical since the forces transmitted through the feet are the primary drivers generating structural vibrations of the top and bottom [39]. The bridge position and loading conditions are critical factors in determining both the static deformation patterns and the dynamic response of the soundboard, since the bridge acts as the primary transmitter of energy from the strings to the plate [40].

The goals are:

- Quantify the stress concentration zones induced by the shape and the location of f-holes;
- Measure and compare the vertical displacement u_z along the central longitudinal axis of the top plate;
- Evaluate correlations between geometric parameters (area and perimeter of f-holes) and mechanical response.

  This type of analysis is essential in violin acoustics because excessive deformation can affect sound quality, and high stress zones can increase the risk of cracks.

2.3.1. Stress study

The internal stress field is governed by the equilibrium equation in the absence of body forces:

$$\nabla \cdot \boldsymbol{\sigma} = 0$$

where $\boldsymbol{\sigma}$ is the Cauchy stress tensor.

COMSOL solves this equation using a Finite Element Method, employing the weak form of the elasticity equations. The constitutive relation for a linear orthotropic material is

given by:

$$\boldsymbol{\sigma} = \mathbf{C} : \boldsymbol{\varepsilon}$$

Where:

- $\mathbf{C}$ is the stiffness tensor for orthotropic elasticity (9 independent constants),
- $\boldsymbol{\varepsilon}$ is the strain tensor, defined as:

$$\boldsymbol{\varepsilon} = \frac{1}{2}\left(\nabla \mathbf{u} + (\nabla \mathbf{u})^T\right)$$

with $\mathbf{u}$ being the displacement vector field.

This formulation enables accurate computation of stress along the three principal axes (longitudinal, radial, and tangential). The simulation revealed that the most significant stress concentrations appear near the inner edges of the f-holes, particularly around sharp curvatures, where stress singularities may arise due to geometrical discontinuities. These zones represent structurally critical regions that are likely to degrade first under prolonged loading.

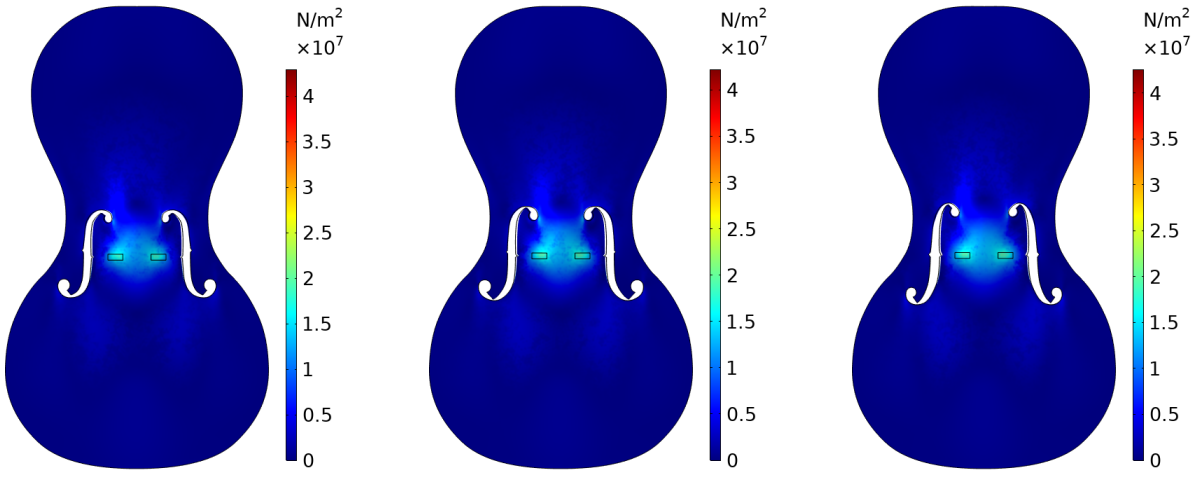

(a) Amati (b) Stradivari (c) Maggini

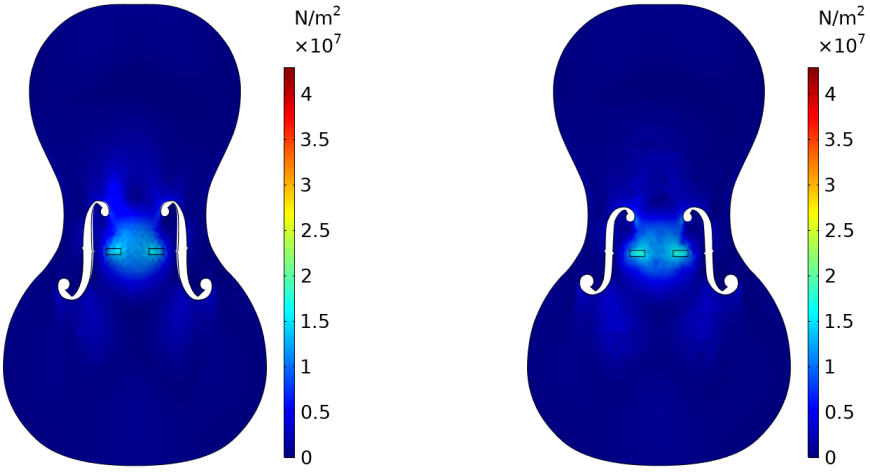

(d) Guarnieri (e) Stainer

Figure 2.5: Effect of the static load of the strings in the violin top plate with different f-hole designs.

2.3.2. Center line displacement study

The vertical component of the displacement field u_z was extracted along the central longitudinal line of the plate. This curve provides a direct measure of the global deformation of the plate under load, which influences both playability and acoustic performance.

The displacement field is obtained by solving the elasticity PDEs under static loading. In

COMSOL, this corresponds to minimizing the potential energy via the weak form:

$$\int_{\Omega} \delta\boldsymbol{\varepsilon} : \boldsymbol{\sigma}\, d\Omega = \int_{\partial\Omega_t} \delta\mathbf{u} \cdot \mathbf{t}\, dS$$

In this study, the force $\mathbf{t}$ was applied downward in the bridge region, and $\mathbf{u} = 0$ was enforced at the plate boundaries.

The mesh used in this study was an extra-fine tetrahedral mesh, which allows accurate resolution of curvature effects and stress concentrations around the f-holes. Mesh refinement was especially important to ensure convergence of the maximum displacement values.

Once the central line displacement curves for each f-hole model were extracted, the maximum displacement values were compared against the geometric characteristics (area and perimeter) of each f-hole type.

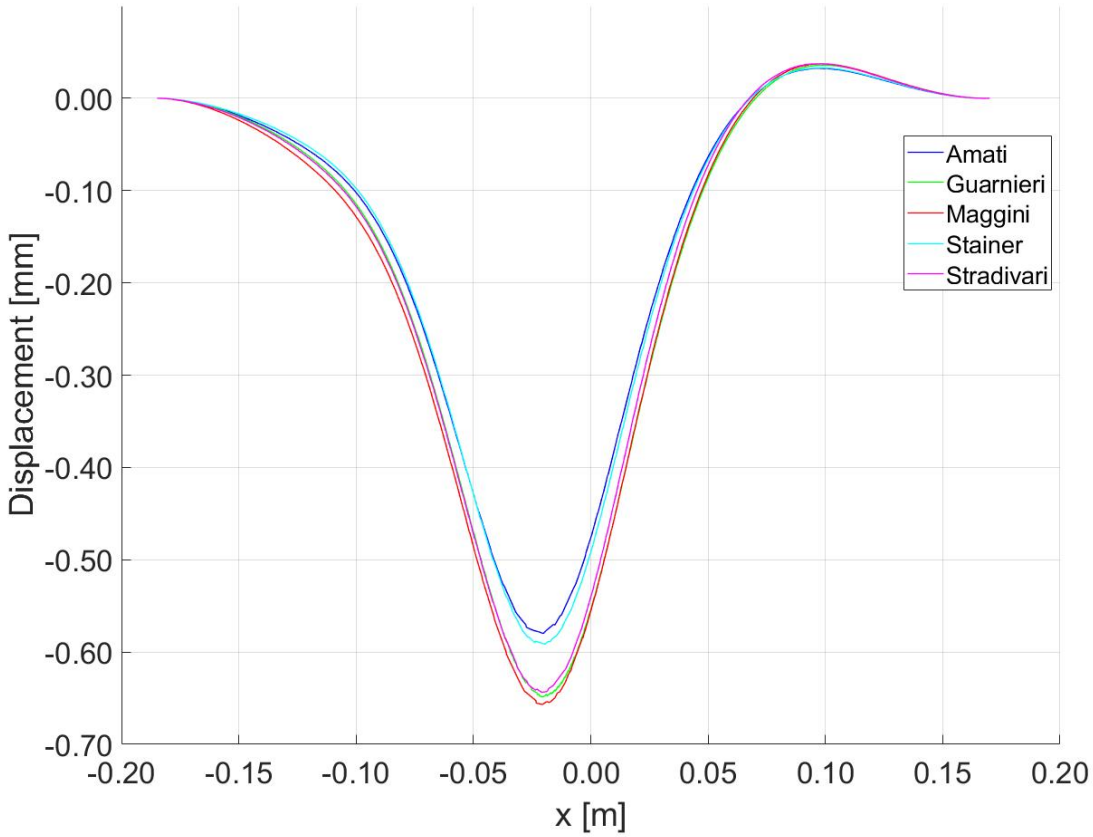

Figure 2.6: Top plate's central line maximum displacement for five f-hole designs.

To understand the correlation between area/perimeter and maximum strain along the center line, two scatter plots were created. Subsequently, a linear fit was applied and R^2

was calculated. In doing so, it was possible to verify the linear trend of the data.

The next study aims to test the relationship between the area and perimeter of different f-hole designs and the maximum displacement on the centerline of the plate. The values used were first computed and then displayed in a scatter plot.

f-hole design	Amati	Guarnieri	Maggini	Stainer	Stradivari
Area $[mm^2]$	533.88	637.68	604.25	586.01	590.67
Perimeter $[mm]$	220.48	245.46	240.00	226.49	245.07

Table 2.2: Computed values of area and perimeter of different f-hole designs.

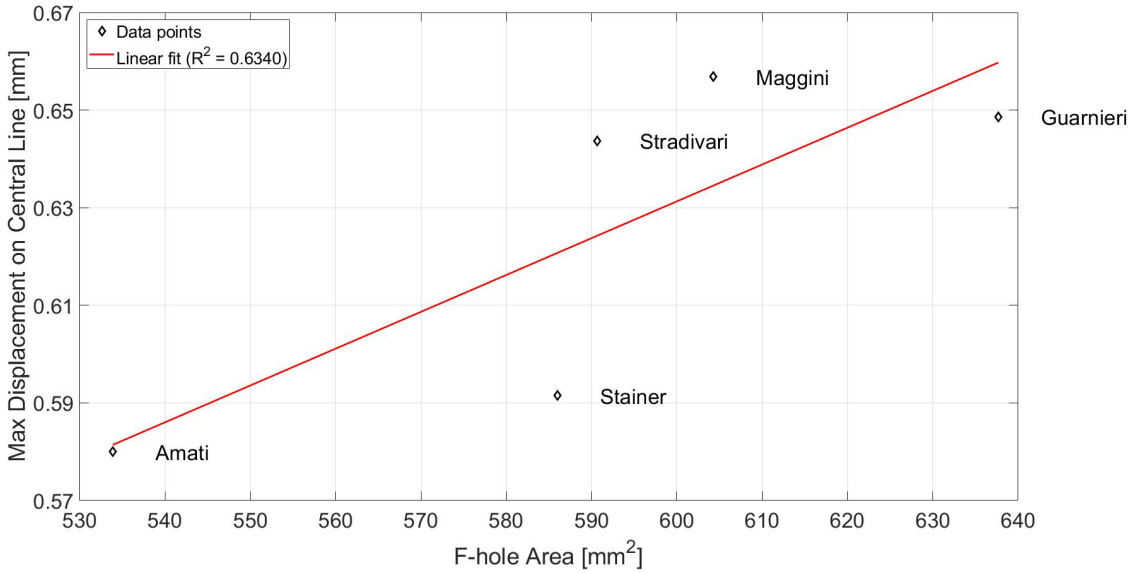

Figure 2.7: Maximum displacement vs f-hole area.

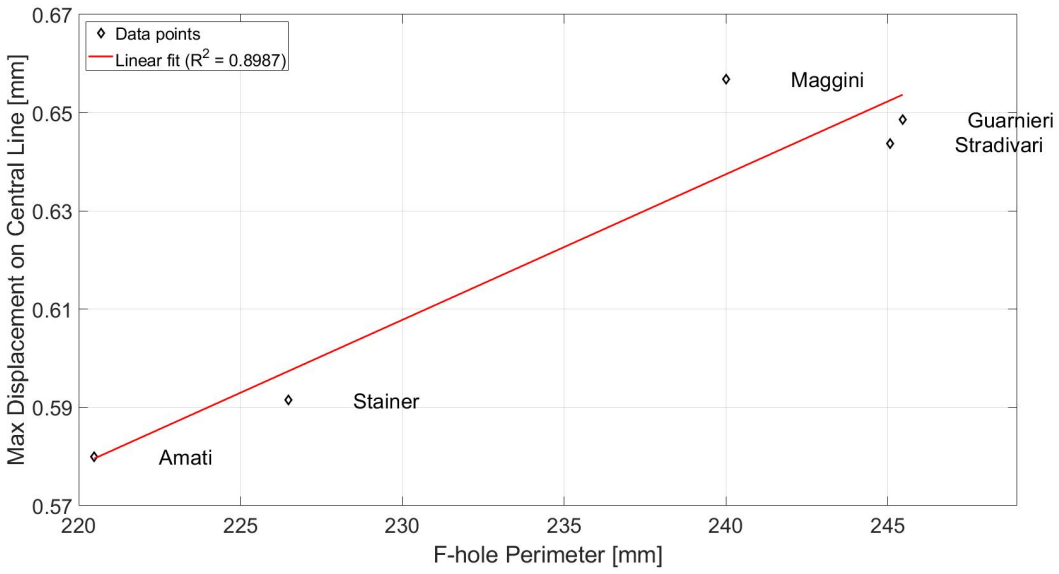

Figure 2.8: Maximum displacement vs f-hole perimeter.

The findings suggest that larger perimeters and areas are generally associated with increased deformation, indicating a trade-off between aesthetic/acoustic openness and mechanical stiffness. This insight is valuable for engineers and instrument designers who want to optimize sound without compromising structural performance.

Looking at the value of R^2 calculated for each scatter plot, we can conclude that the linear fit is better for the perimeter than for the area. This means that there is a more linear correlation in the former case than in the latter case, which implies that the perimeter is a better parameter to linearly define the growth of the displacement. This finding is consistent with classical circuit-analog models of the violin, where the f-hole geometry defines the acoustic inertance, a parameter governing air flow through the openings [41]. In these models, the structural integrity of the top plate represents the mechanical compliance of the system; our results suggest that the perimeter, by governing the local reduction in stiffness, acts as a primary geometric bridge between the static structural response and the functional acoustic parameters. Relative to area, the value of R^2 advises us that there may be other parameters that influence the maximum strain on the center line.

2.4. Mechanical role of f-holes

To evaluate the influence of f-hole geometry on the mechanical performance of the soundboard, a comparative analysis was conducted between two extreme cases: the Amati model, characterized by the smallest perimeter of those examined, and the Guarneri

del Gesù model, which has the largest perimeter. Historical experimental studies have suggested that the f-hle configuration significantly influences the overall response of the instrument [42]. Although these observations primarily referred to the vibroacoustic response, they also raise a fundamental structural issue. The analysis focuses on the stress distribution across the top plate and the displacement fields along each of the three principal directions (x, y, z), providing a comprehensive picture of the mechanical response under identical loading conditions. Comparative visualizations were generated to facilitate direct comparison, with the left half of each plot representing the Amati model and the right half showing the Guarneri configuration.

2.4.1. Stress distribution

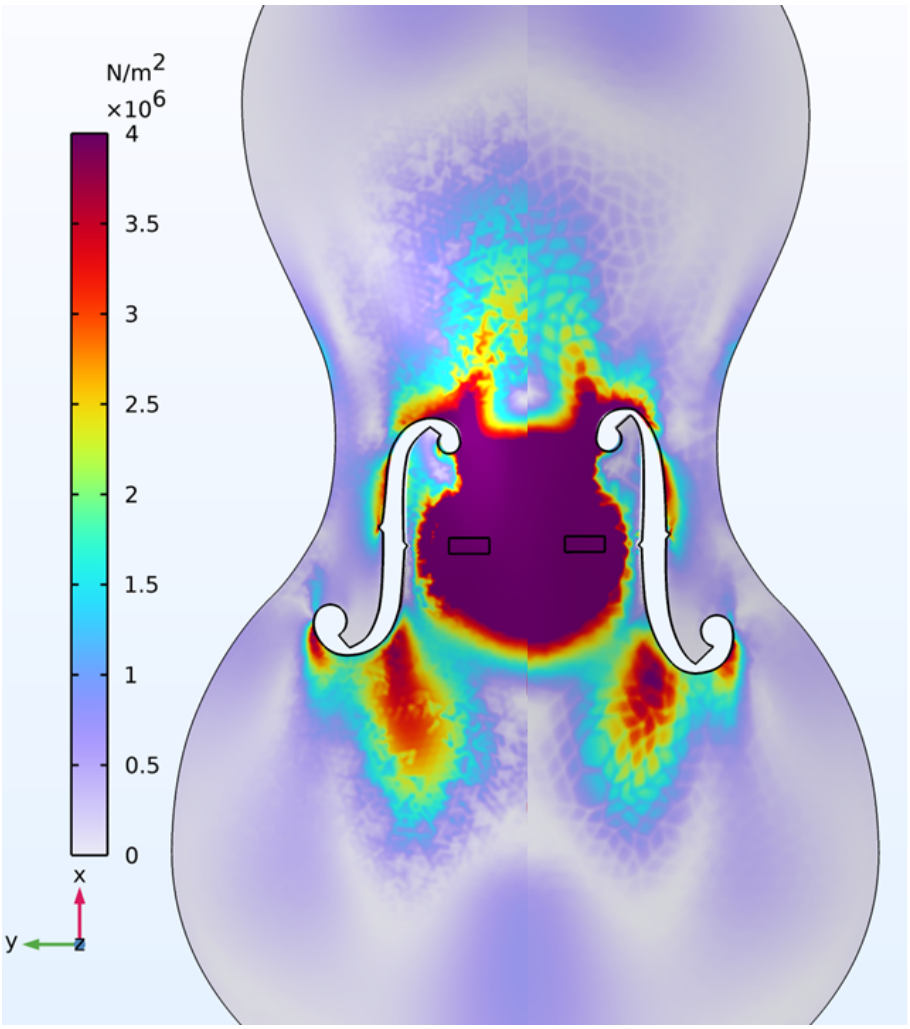

Figure 2.9: Amati-Guarnieri stress comparison plot

Analysis of the stress distribution on the soundboard reveals maximum values in the order of $4 \cdot 10^6 \mathrm{N/m^2}$ for both models considered. The maximum stress zones are concentrated in the central region of the soundboard near the bridge and in the areas immediately adjacent to the upper and lower tips of the f-holes, where localized stress concentrations occur. A direct comparison between the Amati model (f-hole perimeter: 220.48 mm) and the Guarneri del Gesù model (f-hole perimeter: 245.46 mm) shows that the maximum stress values remain essentially unchanged. The critical stress zones are found in the same locations in both models, indicating that the variation in the opening perimeter equal to 24.98 mm (10.2% of the smaller perimeter) does not alter the location of the most stressed regions. The main observation concerns the spatial distribution of stress: while peak values are comparable, the extension of the high-stress zones shows slight variations in the distribution without substantially altering the overall mechanical behavior of the structure. Therefore, no evidence emerges that justifies an intrinsic mechanical advantage of one model over the other in terms of structural strength, confirming that both configurations are equivalent in terms of maximum stresses induced by the applied load.

2.4.2. Displacement on the xy plane

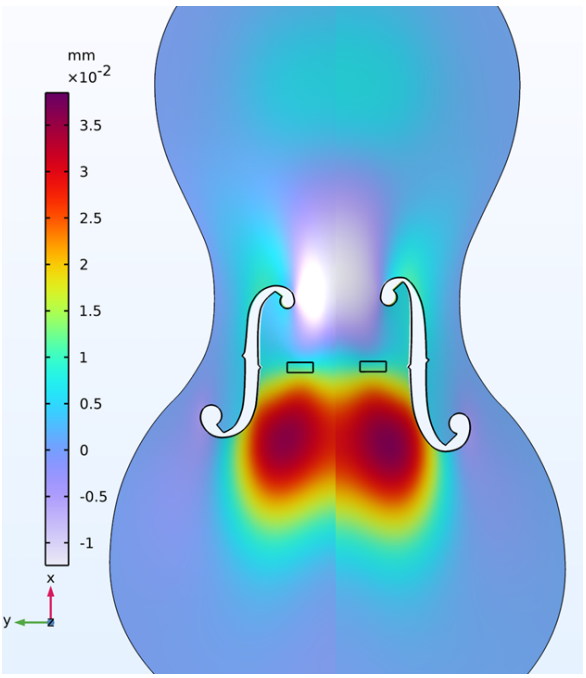

Figure 2.10: Amati-Guarnieri x displacement comparison plot

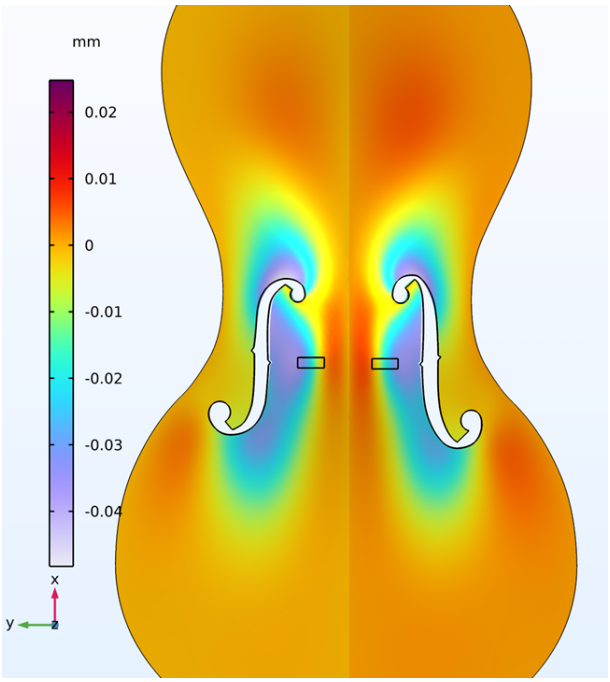

Figure 2.11: Amati-Guarnieri y displacement comparison plot

Starting from the observation of the displacement along the x-axis, longitudinal to the

grain of the soundboard wood and parallel to the axis of the instrument, a distribution characterized by values ranging from $-1 \cdot 10^{-2}$mm to $4 \cdot 10^{-2}$mm is observed. In response to the vertical load applied to the bridge pins, the top plate exhibits complex in-plane deformation. The plots show that the central region, below the load area, exhibits the maximum positive values, while the upper area exhibits negative values. The perimeter areas assume displacement values around 0 mm, respecting the boundary conditions imposed by the coupling of the top plate with the side ribs.

The displacement along the y-axis, orthogonal to the longitudinal axis of the instrument and the wood grain, reaches values in the range from $-5 \cdot 10^{-2}$mm to $2.5 \cdot 10^{-2}$mm. As with displacement along the x-axis, the most stressed area of the soundboard is the one surrounding the loading area. In particular, the central region exhibits positive values, while the areas adjacent to the f-holes show the most marked negative values. This pattern highlights how the location of the loading area represents a transition zone between positive and negative displacements along the y-axis. The areas adjacent to the inner edge of the f-holes assume the lowest values, demonstrating how the openings locally modify the stiffness of the structure and allow differential deformations, helping to shield the perimeter areas and maintain their stability.

The comparison between the Amati model and the Guarneri del Gesù model for both displacement components in the xy plane demonstrates that the variation in the perimeter of the f-holes does not significantly alter the mechanical response of the soundboard in the analyzed plane. The displacement distributions, both for the x- and y-axis couples, are identical, with regions of maximum and minimum displacement located in the same positions and ranges of comparable values. The displacement in the xy plane therefore remains substantially unchanged within this range of variation in the perimeter of the openings, indicating that this range of geometric variation does not significantly influence the planar stiffness of the structure. Previous studies have shown that the primary role of the f-holes is to couple the internal air volume with the ambient air to control air resonance. This is consistent with the observed mechanical similarity, suggesting that, within the constraints of classical violin making, the design of the f-holes is optimized to fulfill its acoustic purpose while maintaining the overall structural integrity of the soundboard [43].

2.4.3. Displacement along the z-axis

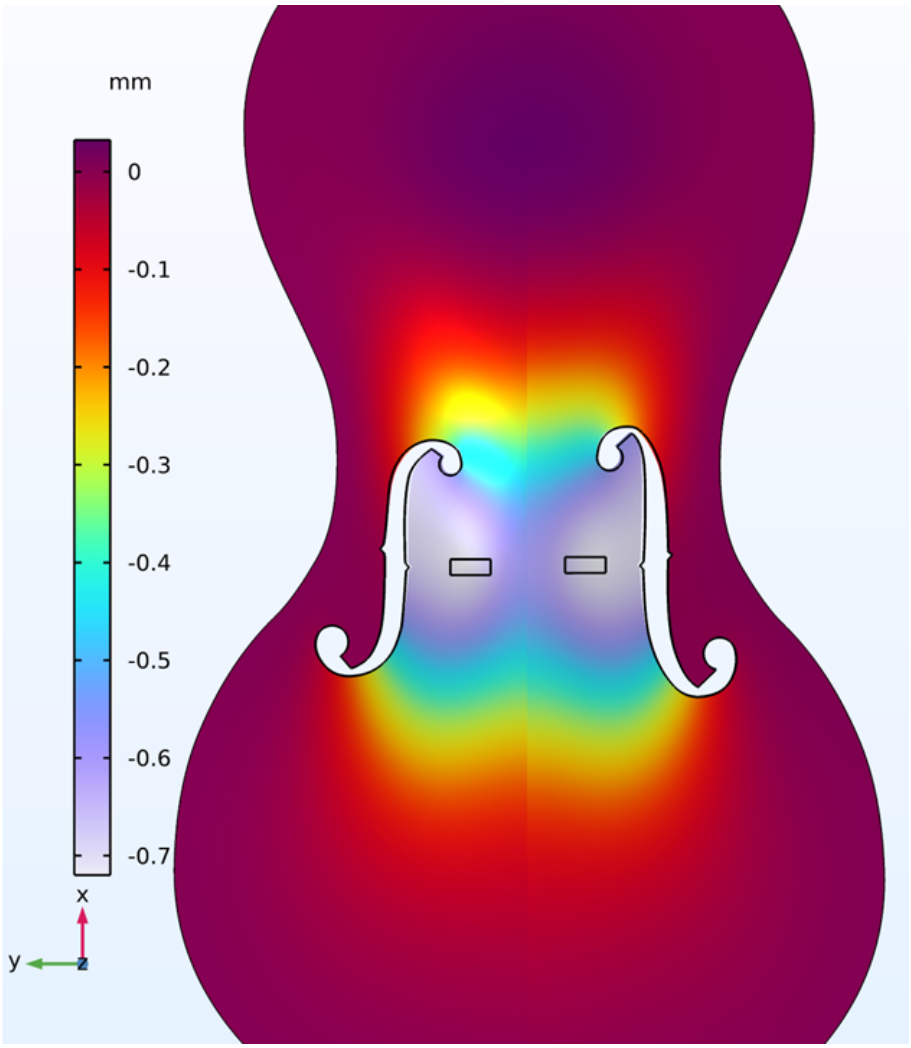

Figure 2.12: Amati-Guarnieri z displacement comparison plot

Analysis of displacement along the z-axis, perpendicular to the plane of the top plate, reveals a mechanically relevant aspect of the role of f-holes in the structural response of the top plate. The plots highlight clear differences in behavior between various areas of the top plate. As with the xy-plane, deformations along the z-axis are concentrated around the load-bearing area on the bridge, reaching maximum negative strain values. The central region of the instrument deflects under the vertical load, exhibiting flexural behavior. In contrast, the perimeter areas of the soundboard maintain displacements around 0 mm. The isolation effect introduced by the f-holes represents a fundamental element for the mechanical functionality of the violin. From a mechanical point of view, this ensures a response to load while respecting the boundary conditions imposed by the

ribs, allowing the central region to vibrate more freely and with greater amplitudes than the perimeter zones. The central area of the soundboard can, therefore, oscillate at specific frequencies without compromising the actual boundary conditions. The f-holes effectively decouple the central vibrating region from the constrained edges, as explained in acoustic studies [44], where the openings introduce compliance that allows the bridge-island region to vibrate more freely while the perimeter remains coupled to the sides, creating distinct vibration zones, crucial to the instrument's sound production.

The comparison between the two reference models confirms that, despite the variation in the f-hole perimeter, both configurations exhibit similar mechanical characteristics, corresponding critical zones, and comparable deformation values. Therefore, varying the perimeter of the openings does not introduce different displacement patterns, but this analysis highlights the shielding effect that allows the perimeter stability of the top plate to be safeguarded. The out-of-plane deformation ranges from approximately -0.7 mm in the central region to values close to 0 mm at the perimeter, resulting in a deformation ratio of approximately 7:1 between the central and edge regions. This pronounced difference demonstrates the effectiveness of f-holes in mechanically isolating the central vibrating region from the constrained perimeter.

2.4.4. Mechanical implications of f-holes on the top plate

The vibrational response of the violin is strongly influenced by the local stiffness of the bridge area [18]. The steady-state analysis illustrates how the f-holes modify this stiffness, acting as a mechanical release that effectively decouples the central vibrating island from the constrained perimeter.

From a structural perspective, the introduction of free internal edges defines two distinct zones: the bridge island, characterized by greater vibrational freedom, and the perimeter zone, which adheres to the rigid boundary conditions imposed by the ribs. As observed in the literature, the removal of material alters the stiffness distribution and modal patterns [45]. Although experimental studies suggested that specific variations in the f-hole style played a dominant role in the mechanical response [42], FEM results indicate the opposite under static loading. Despite the difference in perimeter between the two historical designs, the observed stress distributions and displacement fields are comparable. This suggests that, while the existence of the f-holes is crucial for mechanical release, variations in their geometry play a secondary role compared to the overall rigidity of the top plate. Consequently, the mechanism by which the f-holes limit direct stress transfer appears to be independent of the specific design.

In summary, f-holes act as a functional element that allows the necessary acoustic communication between the internal cavity and the exterior, while also regulating the distribution of mechanical stresses on the soundboard. This confirms that the structural integrity of the violin soundboard is preserved throughout the spectrum of traditional Cremonese designs.

3 | BEM Analysis

Following the FEM simulation, a simulation based on the Boundary Element Method (BEM) in COMSOL was then performed. The objective is to identify how the different f-hole designs influence the sound pressure and acoustic power radiated by the musical instrument. Unlike FEM simulation, which requires domain discretization, BEM focuses only on the surface of the radiator, making it very suitable for sound propagation simulations in a non-limited medium such as air. Through the coupling between FEM and BEM simulation through COMSOL Multiphysics, it was possible to search for a relationship between the vibrational modes and the acoustic radiation patterns for each type of design.

3.1. Geometry and Material

For the BEM simulation, a complete violin cornerless model was used, created on Autodesk Fusion, and imported into COMSOL via STEP file.

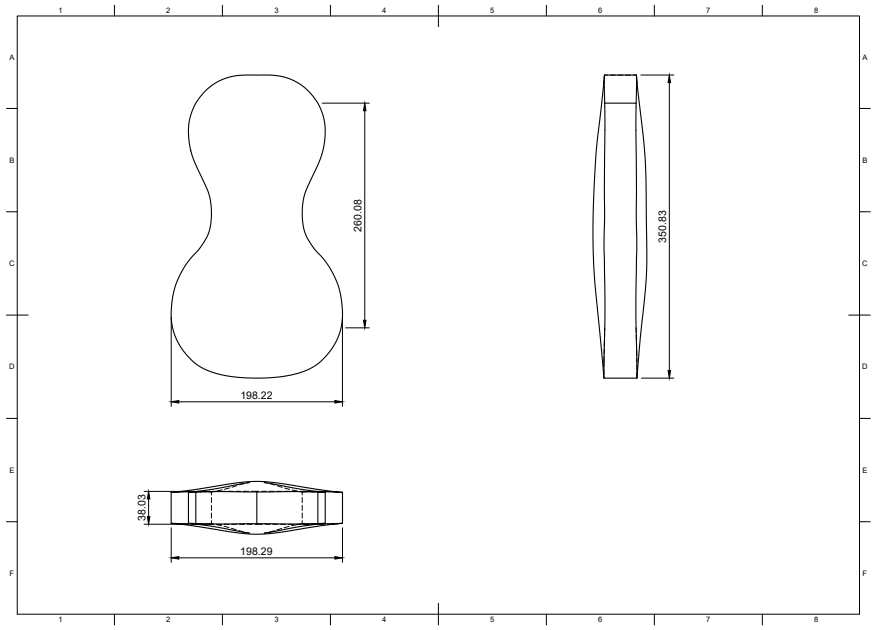

Figure 3.1: Cornerless violin full body model.

The full body of the violin includes only orthotropic materials, but of different types. In particular, the material assigned to the top plate is orthotropic spruce, while that assigned to the ribs and back plate is orthotropic maple. As previously documented [46], the mechanical properties of wood can vary significantly depending on moisture content and grain orientation; however, the orthotropic model used captures the fundamental anisotropy required for accurate vibration predictions.

3.1.1. Material properties

Material	Density [kg/m^3]	Young's Modulus [MPa]			Shear Modulus [MPa]			Poisson's Ratio		
	ρ	E_{L}	E_{R}	E_{T}	G_{LR}	G_{RT}	G_{LT}	ν_{LR}	ν_{RT}	ν_{LT}
Spruce	402	12000	925	737	695	217	653	0.38	0.51	0.50
Maple	586	9100	1329	1147	1475	425	842	0.49	0.66	0.65

Table 3.1: Material constants. In the subscripts, L refers to the longitudinal component, T to the tangential component, and R to the radial component. Source: [4]

The properties of the two materials assigned to the model directly influence the vibrational and acoustic behavior of the instrument. The spruce, assigned to the top plate, has properties that allow for efficient vibrations, transforming mechanical energy into air movement, improving the dynamic response and achieving smooth and controlled sound propagation. The maple used for the ribs and the back plate has a higher density and greater overall rigidity than spruce. This allows the back to support and reflect vibrations from the top plate, increasing overall structural stability. The combination of these two materials maximizes radiating capacity and dynamic response while maintaining rigidity and structural support.

3.1.2. Fluid-structure coupling

The transfer of mechanical energy from the violin body to the surrounding air is governed by the fluid-structure coupling conditions at the interface. This interaction is based on the principle of action-reaction and the continuity of normal displacements, ensuring that the inviscid fluid remains in contact with the vibrating surface in the normal direction. In the present model, the normal velocity of the violin surface acts as a pressure source, satisfying the compatibility conditions required for the solution of the Helmholtz equation in the acoustic domain [47]. Then a spherical volume with a radius of 1 m was defined around the violin, representing the region of air in which the sound propagates. The surface of this sphere is the study domain of the acoustic pressure, derived from the integration of

the surface itself. The coupled FEM-BEM approach used in this study addresses the need to consider the interaction between structural vibrations and the enclosed air volume. As demonstrated by finite element simulations of several string instruments, the internal air has the dual effect of lowering the natural frequencies and altering the order of the mode shapes compared to simulations of the structure alone [26]. Therefore, modeling the acoustic domain is a crucial step to ensure that the simulated radiation results reflect the actual physics of the instrument.

Material	Density [kg/m^{-3}]	Speed of sound [m/s]
Air	1.2	343

Table 3.2: Standard air material constants

To discretize the violin's domain, a mesh with quadratic order elements was adopted. Numerical studies have shown that the use of quadratic shape functions offers substantial advantages in terms of accuracy compared to linear approximations, reducing the relative error in determining the far-field sound pressure [48].

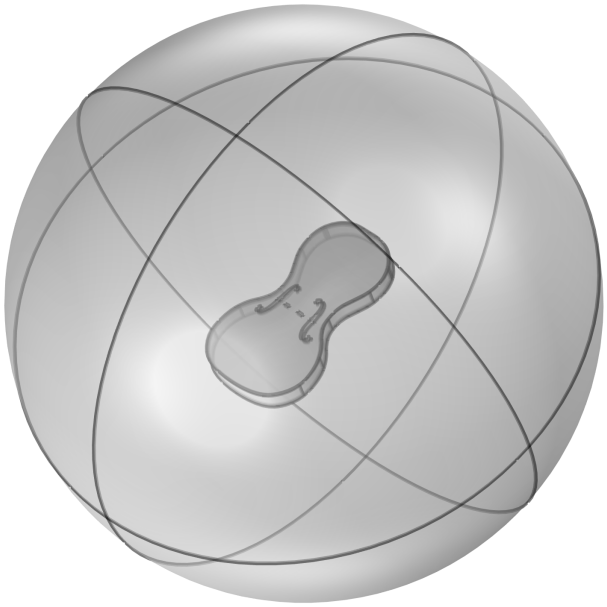

Figure 3.2: Model of a violin immersed in a sphere of air

3.2. Eigenfrequencies study

As in the case of the FEM analysis, the first step of this second study is the identification of the eigenfrequencies and vibration modes.

Following the eigefrequencies study conducted on the complete violin, the modes with the highest standard variation were identified, which highlight the frequencies or frequency ranges in which there is a greater vibrational difference between the different f-hole designs. Recent coupled FEM-BEM simulations on historical violins have successfully predicted signature modes validating the methodology for parametric studies where geometric variations, such as f-hole design, are systematically examined [49].

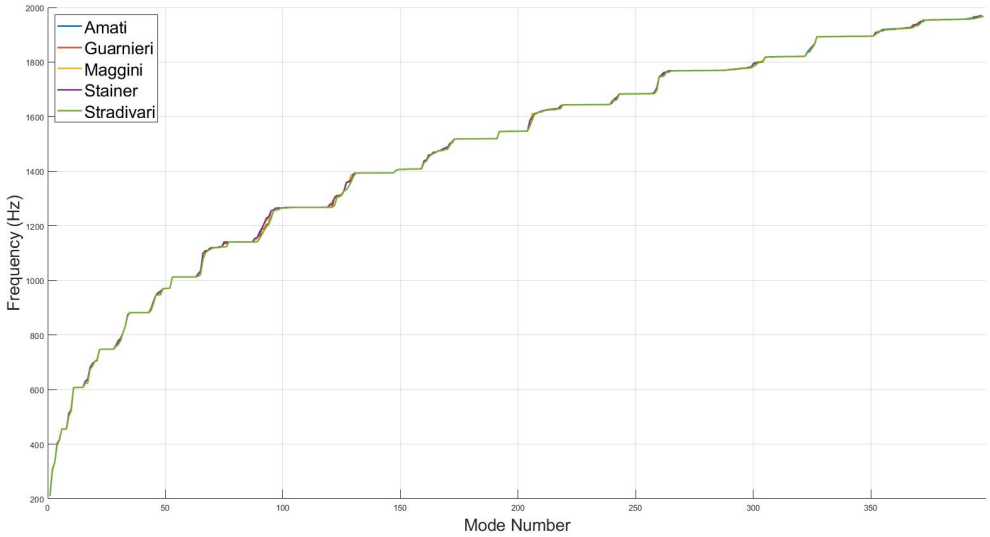

Figure 3.3: Full body eigenfrequency variation

For a better visualization, the eigenfrequencies normalized with respect to the Amati model taken as a reference have been plotted.

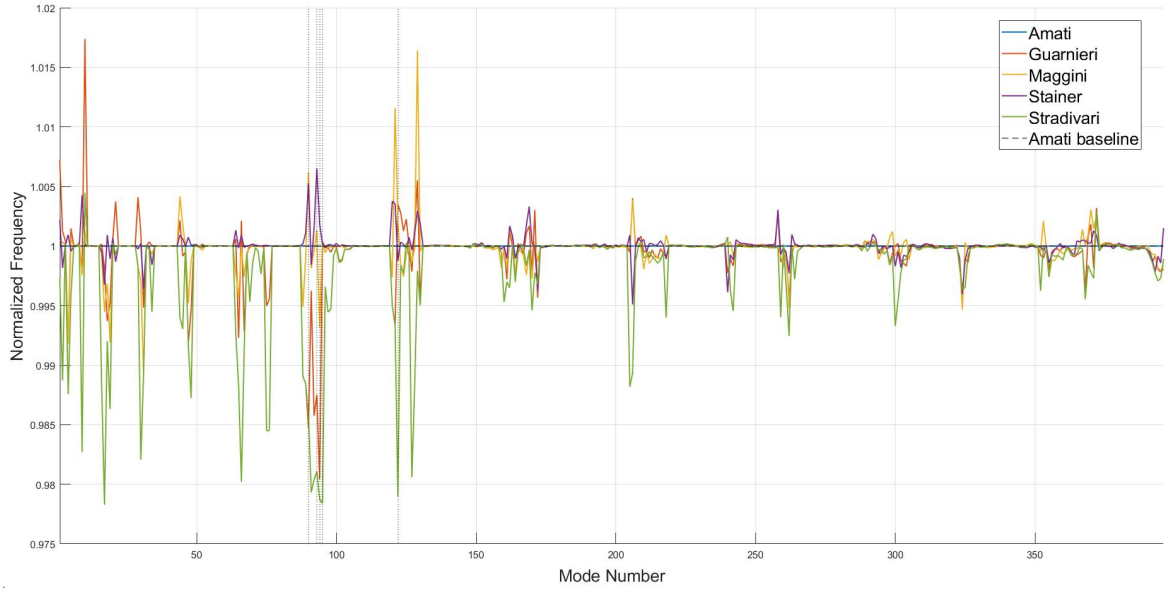

Figure 3.4: Normalized eigenfrequencies (relative to Amati)

Mode	94	122	93	90	95
$Mean$[Hz]	1220.4	1298.0	1214.5	1165.6	1249.2
$StdDev$[Hz]	13.30	13.06	12.91	12.23	12.23

Table 3.3: 5 modes with maximum standard deviation

The majority of modes with the highest standard deviation are between the 90th and 95th modes and correspondingly at frequencies between 1165.6 Hz and 1249.2 Hz. These observations support the hypothesis that the f-hole design not only affects the plate's mechanical response but also has a potential impact on its vibrational properties. The next step focuses on the eigenfrequency analysis to further investigate these relationships in the modal domain.

3.3. Sound Pressure Level (SPL) study

After identifying the natural frequencies, the analysis continues with the study of the violin's vibro-acoustic behavior using the COMSOL Multiphysics node. In this phase, the interactions between the structural vibrations and the surrounding acoustic field are simulated using a coupled FEM–BEM approach, which allows for the determination of sound propagation and radiation. COMSOL's integrated Multiphysics approach thus allows for the simultaneous analysis of the mechanical and acoustic responses of the system, providing information on radiated power and sound pressure distribution.

3.3.1. SPL calculation

In practice, the BEM simulation was performed using the complete violin model previously analyzed with the FEM method. The violin's solid domain was coupled to an acoustic domain represented by a spherical air region with a radius of 1 m, modeled as an external acoustic domain using the boundary element method. In COMSOL Multiphysics, the structural vibrations obtained from the FEM analysis were used as coupling conditions for the acoustic problem, where the violin's normal surface velocity served as a pressure source in the surrounding air. Solving the Helmholtz equation using the BEM method then provided the external acoustic pressure field for each frequency of interest. From these results, the SPL was calculated and displayed on the surface of the observation sphere as the average of the domain values. SPL plots allow comparison of radiation efficiency between different f-hole designs, highlighting the most significant differences in the frequency ranges corresponding to the main vibration modes.

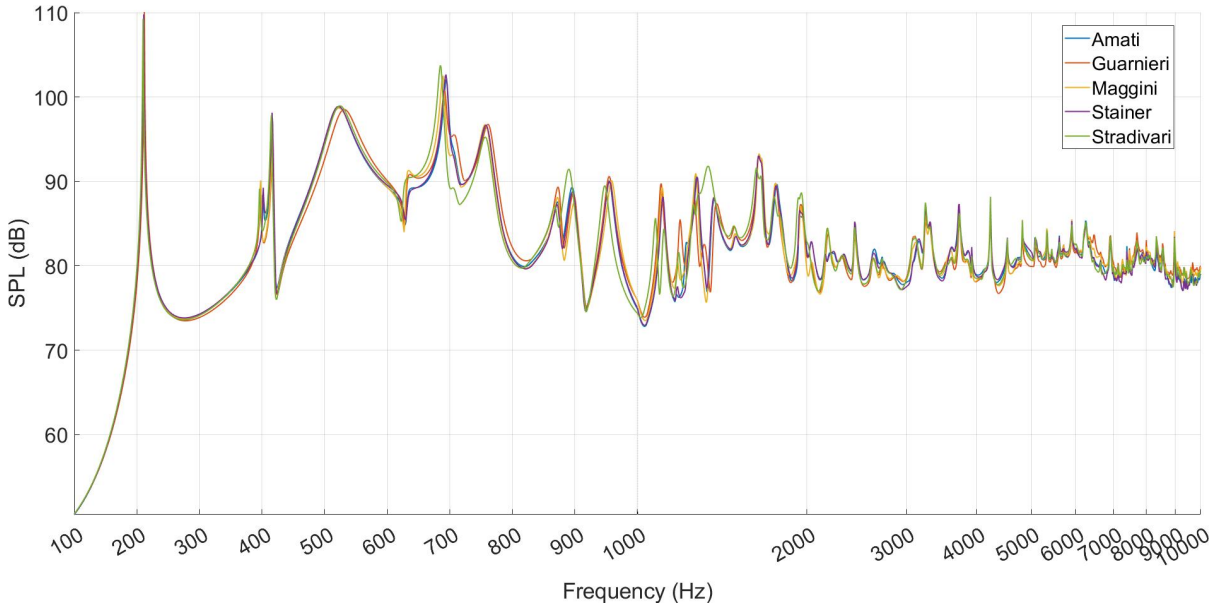

Figure 3.5: SPL different f-holes design

The average SPL was calculated over the surface of the observation sphere used as the external acoustic domain. Knowing that the SPL at a point is defined as:

$$SPL(\mathbf{r}) = 20 \log_{10} \left(\frac{|p(\mathbf{r})|}{p_{\text{ref}}} \right)$$

where $p_{\text{ref}} = 20\ \mu\text{Pa}$ is the reference pressure in air.

Using COMSOL's Surface Average operator it is possible to obtain the average sound pressure value by averaging the arithmetic of the point values of SPL according to the following formula:

$$SPL_{\text{avg}} = \frac{1}{A} \int_A SPL(\mathbf{r})\, dA$$

where A is the total area of the surface of the sphere circumscribing the violin. This averaging procedure follows standard methodologies for determining sound power levels under anechoic conditions, in accordance with ISO 3745:2012. These protocols involve the integration of pressure levels over a spherical measurement surface that completely envelops the source [50]. This approach allows for the characterization of far-field radiation from the instrument independently of the measurement location.

3.3.2. Average SPL and statistical distribution

SPL values were simulated for a linear frequency scale covering the range 100-1000 Hz and consecutively for a logarithmic scale covering the range 1000-10000 Hz. The mean value

of SPL was then plotted over the whole frequency range showing the standard deviation.

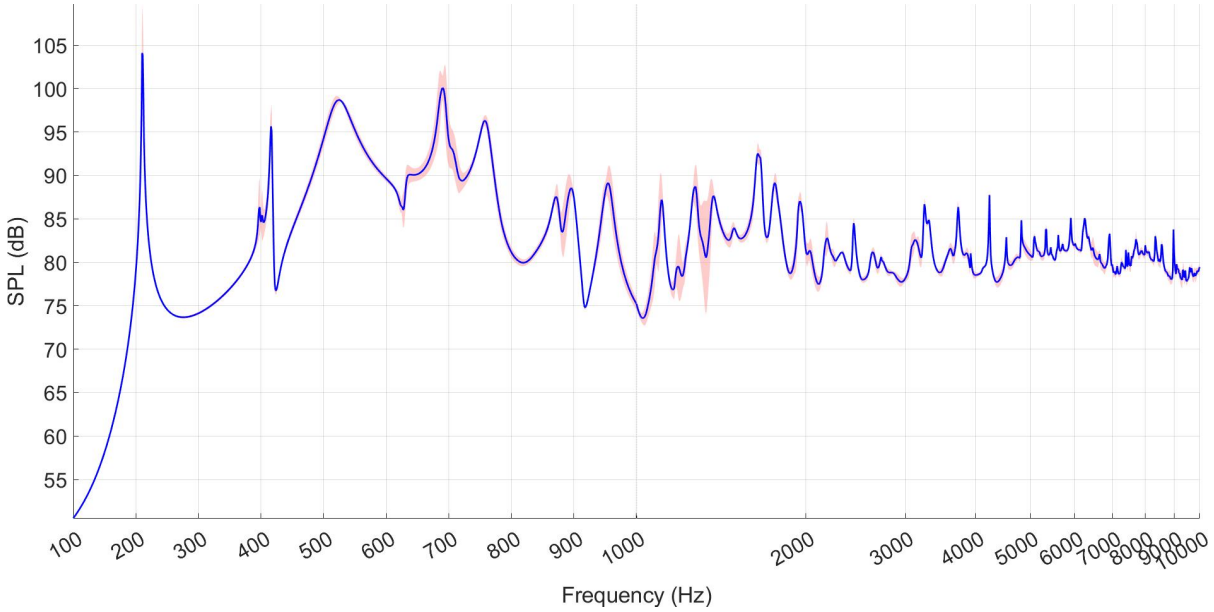

Figure 3.6: Average value of SPL and stadard deviation

To reduce the local oscillations and noise present in the standard deviation data of the SPL analysis, the data were subjected to a Gaussian smoothing algorithm, implemented in MATLAB with the smoothdata function. In particular, this algorithm allows each point of the curve to be replaced with a weighted average of the points around it, thus obtaining a more regular curve without losing data characteristics. By eliminating the noise, it was possible to more precisely identify the points of the SPL curve with the highest standard deviation. Previous studies have shown that the strong coupling between air and wood resonances can lead to rapid changes in acoustic radiation efficiency when geometric parameters are altered [51]. In these critical frequency ranges, even small changes in the design of the f-holes can significantly redistribute energy between the coupled modes, resulting in the high statistical dispersion observed in the standard deviation peaks.

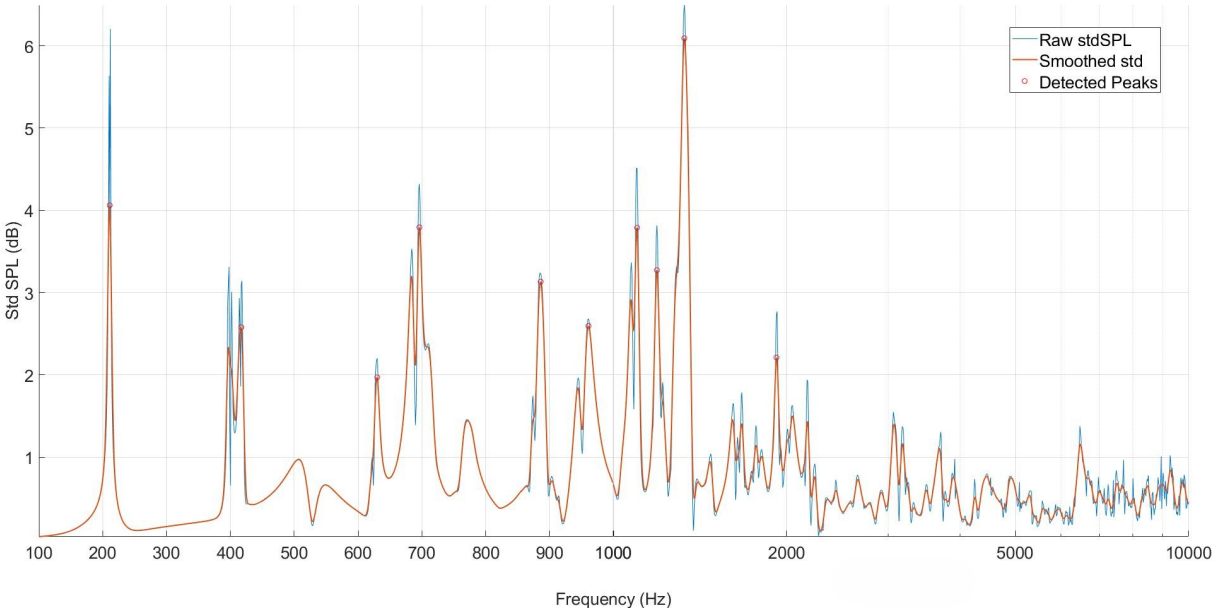

Figure 3.7: Raw vs Smoothed standard deviation SPL and detected peaks

3.3.3. Identification of critical frequencies

Peak	Frequency [Hz]	Peak [dB]	FWHM [Hz]	Half Width [Hz]	Std dev rank
1	211.0	4.061	8.6	4.3	2
2	417.0	2.577	28.2	14.1	8
3	630.0	1.970	9.1	4.6	10
4	696.0	3.793	38.9	19.4	3
5	886.0	3.133	15.1	7.5	6
6	961.0	2.595	21.2	10.6	7
7	1099.3	3.789	50.2	25.1	4
8	1190.0	3.273	31.4	15.7	5
9	1328.4	6.092	75.2	37.6	1
10	1920.1	2.210	48.3	24.1	9

Table 3.4: Top 10 points with highest standard deviation of SPL

The ten points with the greatest SPL standard deviation were identified, and the peak lobe width and semi-width were determined to consider frequency ranges that contribute to the same peak sound pressure. The FWHM (Full Width at Half Maximum) of the 6 largest lobes, equal to 56.30 Hz, was also averaged, with an average half-width of 28.15 Hz. The maximum acoustic variability between different f-hole designs was identified at 1328.4 Hz.

This result is consistent with previous studies, which identify the so-called "bridge hill" between 1000 Hz and 3000 Hz [52] , a spectral region characterized by a high modal density and a strong sensitivity of the sound radiation to the mechanical characteristics of the system, justifying the statistical analysis conducted subsequently. Therefore, observing these points, the frequencies emerge in which the differences in vibrational behavior and acoustic radiation are most incisive. In particular, the results show that the greatest differences between different designs are concentrated between 400 Hz and 1400 Hz, with the main peak corresponding to 1328 Hz, i.e., where the acoustic response has greater variability between different models. Overall, the results suggest that the geometry of f-holes has a quantifiable, but not uniform, impact on acoustic radiation; some frequency bands seem more sensitive to geometric variations in the model and represent the areas of greatest interest for the study. The FHWM values provide valuable information on the frequency distribution of the acoustic contribution of the vibration modes. Low values indicate localized contributions of a reduced frequency range, while high values suggest an overlap of multiple vibration modes resulting in a more widespread variation in SPL. Regarding the results obtained, a higher concentration of lobes can be observed with a high FWHM value in the frequency range between 1000 Hz and 1400 Hz. In this region, the acoustic response of the violin is more complex due to the interaction between different resonances. In summary, the analysis of the parameters considered highlighted the frequency bands most influenced by geometric variations, which are decisive in the characterization and discrimination of the acoustic behavior of the different models.

3.3.4. Acoustic role of f-holes

In this context of acoustic complexity, the five reference models were analyzed to determine to what extent the perimeter of the f-holes influences the average SPL level in the critical band 1000-2000 Hz.

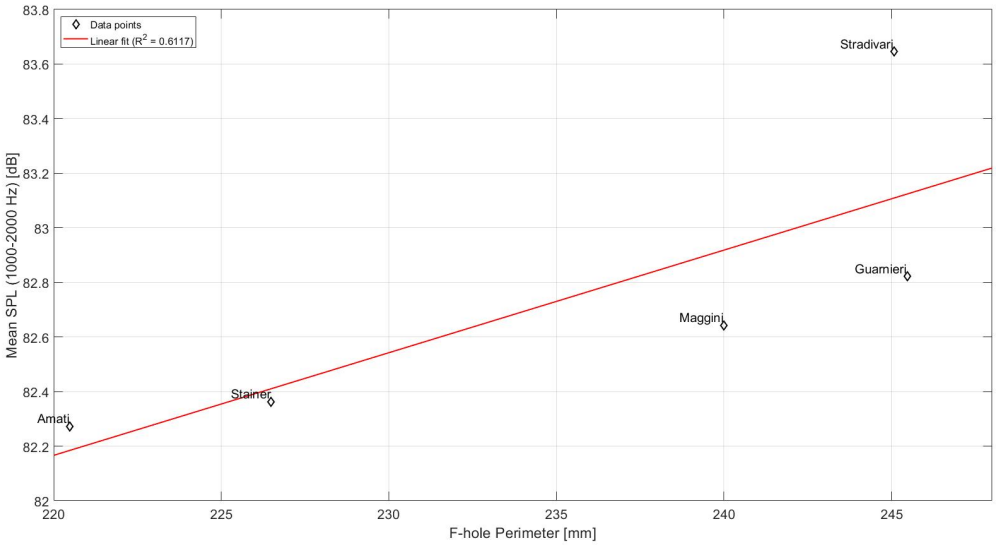

Figure 3.8: Linear Regression Mean SPL vs. Perimeter

3.3.5. Statistical and physical analysis

The linear regression analysis returns a coefficient of determination $R^2 = 0.6117$ and although this value is lower than that found in the mechanical analysis, it indicates that the perimeter is a significant predictor of the acoustic response and useful for increasing it. The decrease in the coefficient R^2 in the transition from the mechanical to the acoustic domain highlights how sound radiation is mediated by additional factors, such as fluid-structure interaction. This observation is consistent with the results of previous studies on archtop guitars, where different f-hole designs analyzed without the air component showed no significant differences. This confirms that fluid-structure interaction is the essential mechanism that drives the acoustic influence of f-hole geometry, distinguishing acoustic results from purely structural behavior [33]. The interpolation line has a positive slope $m = 0.0376$ dB/mm, each 1 mm increase in the perimeter of the f-holes contributes to an increase in the average SPL of 0.0376 dB. The effect produced by a perimeter variation between the Amati (perimeter: 220.48 mm) and Guarnieri del Gesù (perimeter: 245.46 mm) edge cases equal to 24.98 mm would therefore produce a variation in average SPL equal to 0.93 dB which, although small, captures the physical consequences of a change in f-hole design. However, considerable dispersion is evident in the Stradivari model. Despite sharing a comparable perimeter with the Guarneri del Gesù design, the Stradivari exhibits a significantly higher average sound pressure level. This deviation suggests that, while perimeter is a determining factor, acoustic efficiency is also influenced by other construction parameters. Investigating the specific causes of Stradivari's superior

acoustic power requires further analysis that goes beyond the scope of this thesis. In conclusion, the high R^2 value demonstrates that perimeter is a factor governing SPL variability between models. Although the increase per millimeter is small, the precision of this correlation confirms that perimeter is an effective physical lever for determining the instrument's sound power in this frequency range.

4 | Correlation Analysis

4.1. Objective of the correlation analysis

After carrying out the coupled FEM-BEM simulation it is necessary to study the relationship between the natural frequencies of the 5 study models and the acoustic response in terms of SPL. The goal is to identify which ways of vibrating have a significant influence on the value of SPL. More specifically, we want to analyze how different f-hole designs influence the overall acoustic behavior of the instrument.

4.2. Qualitative correlation analysis

From previous studies, we have been able to extract the 5 vibration modes as the greatest standard deviation in frequency for the models considered and the 5 frequencies with the greatest standard deviation of SPL. What we want to highlight is the presence of situations of instability regarding the free frequencies of vibration and the acoustic pressure.

Mode	Mean frequency [Hz]	Std deviation [Hz]	Coeff. variation	Std. Dev. rank
90	1165.6	12.234	1.05%	3
93	1214.5	12.906	1.06%	2
94	1220.4	12.205	1.00%	5
95	1249.2	12.230	0.98%	4
122	1298.0	13.065	1.01%	1

Table 4.1: Top 5 modes with highest standard deviation

Frequency [Hz]	Mean SPL [dB]	Std deviation [dB]	Coeff. variation	Std. Dev. rank
211.0	103.88	4.061	3.91%	2
696.0	97.24	3.793	3.90%	3
1099.3	85.08	3.789	4.45%	4
1190.0	79.38	3.273	4.12%	5
1328.4	80.54	6.092	7.56%	1

Table 4.2: TOP 5 frequencies with highest standard deviation of SPL.

Using MATLAB, a scatter plot was created that represents the points in relation to the standard deviation value relating to the frequencies and the SPL, with marks on the fashions that differ from the others in vibrational and acoustic behavior.

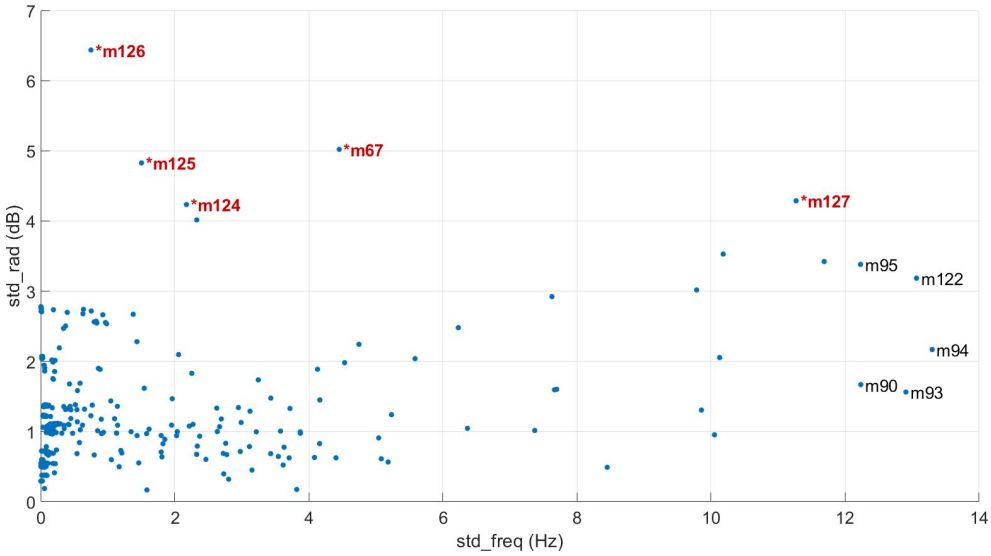

Figure 4.1: Frequency and SPL standard deviation scatter plot

This type of graph allows us to observe the overall behavior of the vibration modes. In particular, the point cloud piled up around the origin highlights a situation in which both the standard deviation values, relating to frequencies and those relating to SPL, remain low and contribute to a general stable behavior. If we move away from this cloud by scrolling through the std dev values we can begin to observe unstable situations, in which the behavior of some specific vibrational modes differs considerably from the general stability. A large value of std freq indicates that the vibration mode varies significantly between different f-hole designs, while a high value of std rad indicates strong variability in sound pressure. Consequently, the points in the graph positioned at the top right represent

the modes that are simultaneously sensitive to the change in design with respect to purely vibrational and acoustic behavior.

To support this, a plot was created that, separately for frequencies and SPL, allows us to observe how many frequencies are within a given range of standard deviation. The peaks close to the origin correspond to the point cloud with stable behavior, the further away from the origin we move, the more dispersion increases, with fewer samples adhering to a certain range of std dev, and the unstable behavior.

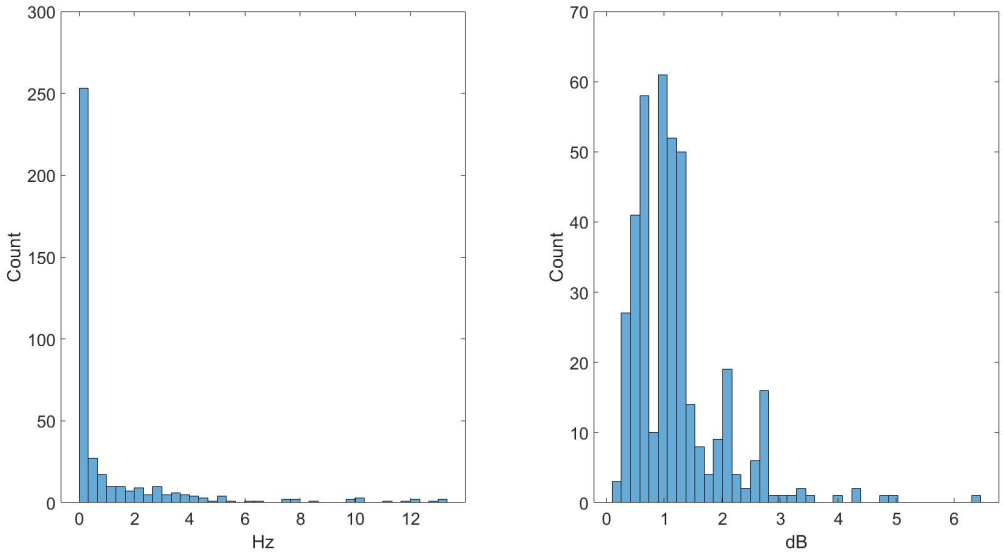

Figure 4.2: Frequencies and SPL standard deviation distribution

A heat map was then created to compare the fashions identified and the points with a high variation of SPL The objective is to identify whether these frequencies contribute to the variation of SPL To do this, the parameter half-width, already calculated previously, was used as a reference distance to determine whether a given frequency belongs to that given lobe in the SPL graph, remembering that the half width parameter used is an average of the half width values of each lobe considered. The average FWHM obtained is 56.30 Hz with a half-width equivalent of 28.15 Hz.

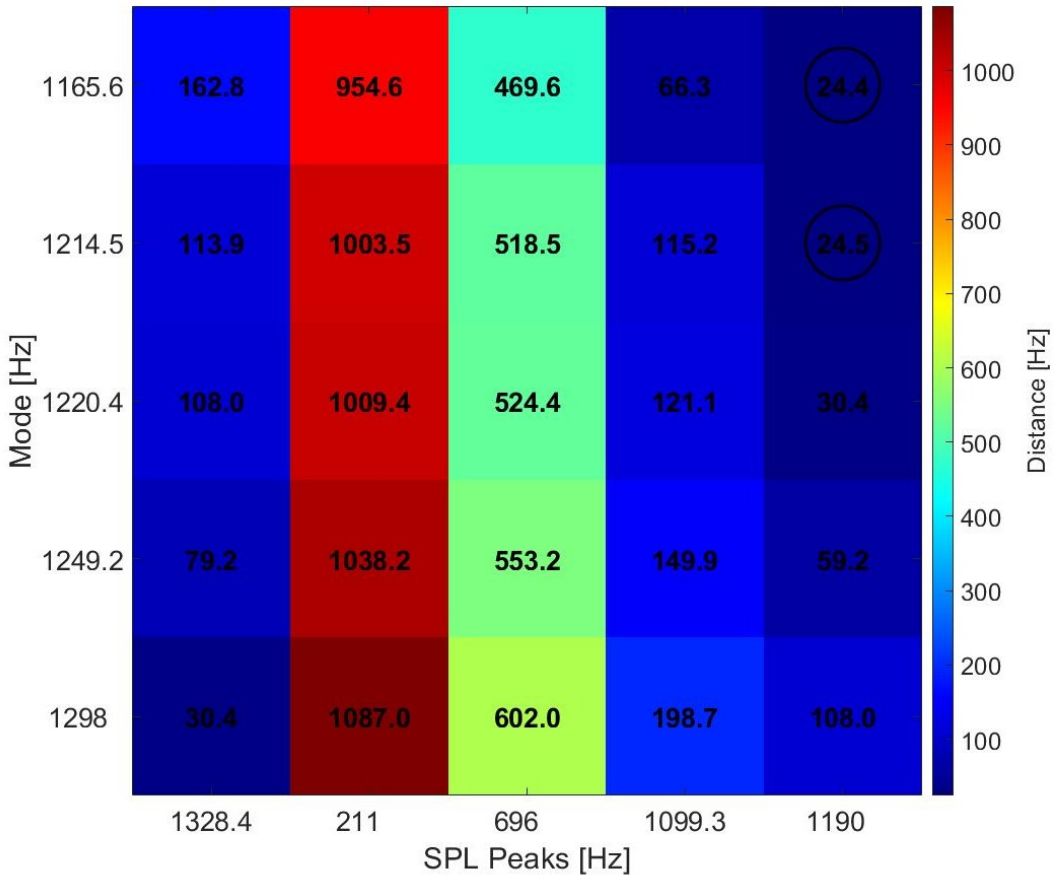

Figure 4.3: frequency distances between vibrational modes and SPL peaks

Low distance values indicate a strong vibro-acoustic coupling and that the sound radiation is dominated in part or in whole by that particular mode, high values instead indicate that the two phenomena do not coincide in frequency and therefore there is a low direct correlation between structural vibration and acoustic response. In particular, observing the heat map, only two points are accepted, which fall within the average half-width reference distance, between 1165.6 Hz and 1214.5 Hz which compete together with the SPL of the lobe at 1190.0 Hz.

4.3. MAC and Mode Switching

Observing the modal shapes, especially those of interest, we realize that they do not coincide perfectly, suggesting the possibility of a phenomenon called "mode switching".

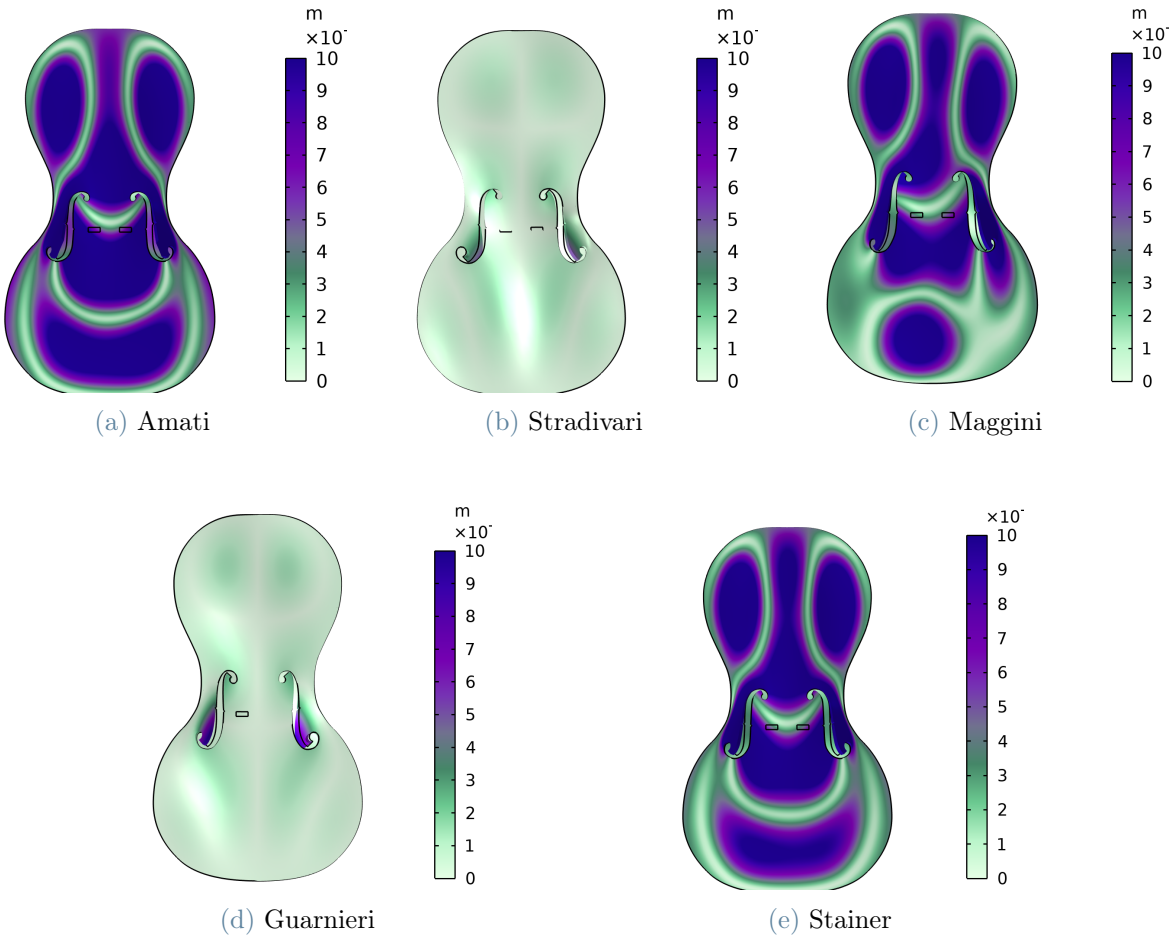

(a) Amati (b) Stradivari (c) Maggini

(d) Guarnieri (e) Stainer

Figure 4.4: Mode 93 shapes for different f-hole designs.

Figure 3.4 shows the mode shape of the 93rd mode for each model. A purely qualitative observation is enough to realize that the situation differs from a theoretical coincidence, indicating the presence of the "mode switching" phenomenon. This phenomenon ,observed then in the analysis of MAC matrices, finds a solid theoretical justification in previous studies on curve veering. In systems dependent on geometric parameters, the eigenvalue curves can tend to approach each other without ever crossing, drastically altering their character and exchanging morphological characteristics [53]. The mode switching occurs in modal analyses when mode shapes differ from each other despite having coincident mode numbers. One would expect each vibration mode to follow a continuous and smooth path in the frequency domain; however, in certain regions, two modes that are close in frequency mutually exchange their characteristics. It is therefore difficult to directly compare modes based solely on their numerical order. To overcome this issue, a similarity measure called the Modal Assurance Criterion (MAC) was introduced to verify whether, despite mode switching, two modes belong to the same type of vibration.

This index is defined as:

$$\mathrm{MAC}_{ij} = \frac{\left|\boldsymbol{\phi}_i^T \boldsymbol{\phi}_j\right|^2}{(\boldsymbol{\phi}_i^T \boldsymbol{\phi}_i)(\boldsymbol{\phi}_j^T \boldsymbol{\phi}_j)} \tag{4.1}$$

where:

- MAC_{ij} is the Modal Assurance Criterion between the i-th and j-th mode shapes, which quantifies their degree of correlation.
- $\boldsymbol{\phi}_i$ is the eigenvector (mode shape) associated with the i-th natural frequency of the structure.
- $\boldsymbol{\phi}_j$ is the eigenvector (mode shape) associated with the j-th natural frequency.
- $\boldsymbol{\phi}_i^T$ denotes the transpose of the vector $\boldsymbol{\phi}_i$.
- $\left|\boldsymbol{\phi}_i^T \boldsymbol{\phi}_j\right|^2$ represents the squared magnitude of the scalar product between the two mode shapes, which measures their directional similarity.
- $(\boldsymbol{\phi}_i^T \boldsymbol{\phi}_i)$ and $(\boldsymbol{\phi}_j^T \boldsymbol{\phi}_j)$ are the quadratic norms of the two modal vectors, used for normalization so that MAC_{ij} is independent of scale.

The MAC ranges from 0 to 1 and allows evaluating the degree of similarity between two mode shapes. A MAC value of 1 indicates that the two mode shapes are identical or perfectly correlated, whereas a MAC value of 0 indicates that the two mode shapes are orthogonal or completely different.

Using MATLAB it was possible to proceed with the calculation of the MAC Matrix. After exporting from COMSOL, for each model and for each calculated self-frequency, the point deformation values of the violin mesh, the mesh points common to all the models were found so as to have a direct and precise comparison between the modes respecting the geometry. For each pair of models the MAC Matrix is then calculated producing an output of 15 matrices (considering the self MAC Matrix).

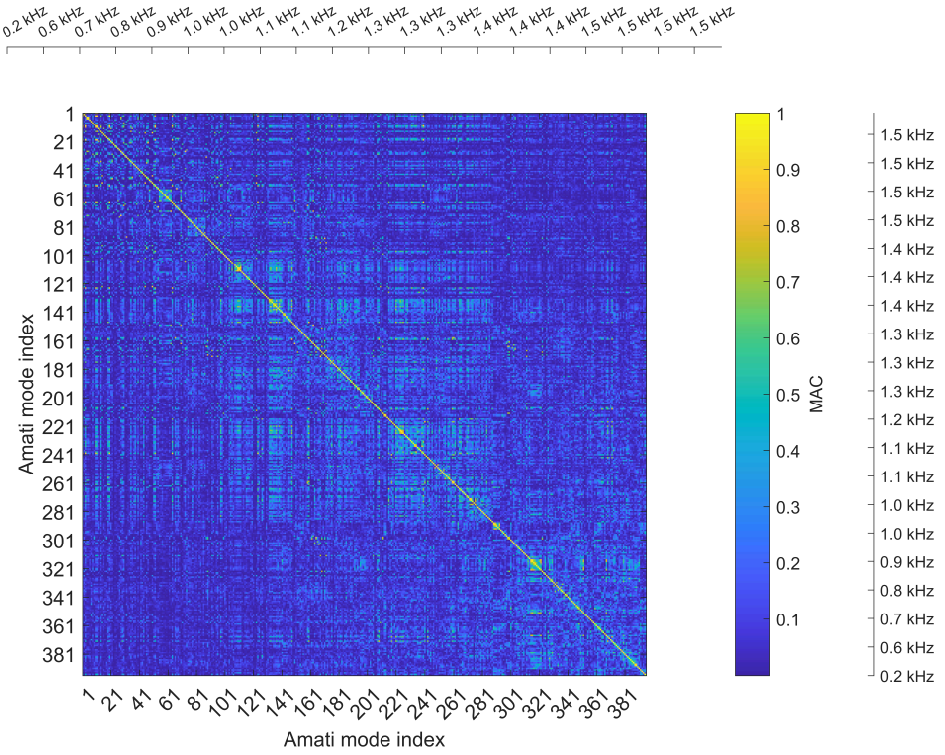

Figure 4.5: Self-MAC matrix for the Amati model

Figure 3.5 represents the self MAC Matrix which relates the modal shapes of the Amati model to itself. The values on the diagonal of the matrix all take on a value of 1, indicating a perfect correlation of the modal shapes of the two theoretical models, which in this case coincide. This shows that the mode data were imported and calculated correctly. Once this is done, the analysis continues with the correlation between different models, an analysis which should highlight the presence or absence of mode switching.

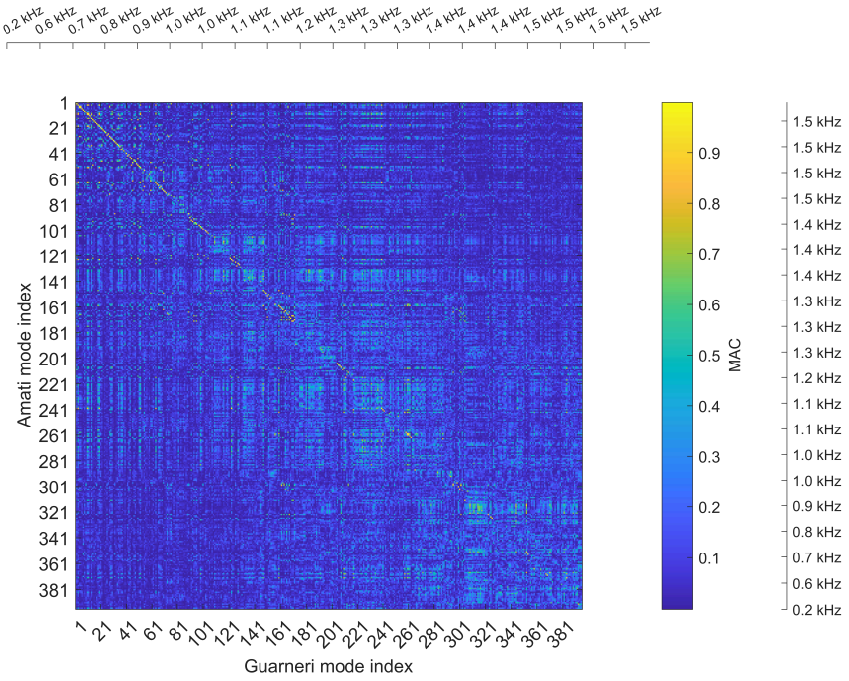

Figure 4.6: Amati-Guarnieri MAC Matrix

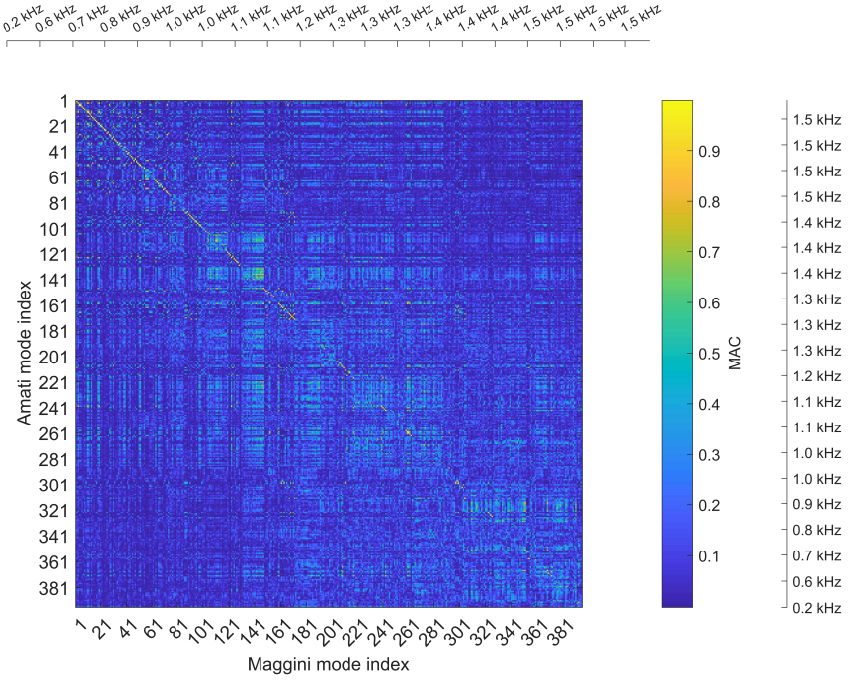

Figure 4.7: Amati-Maggini MAC Matrix

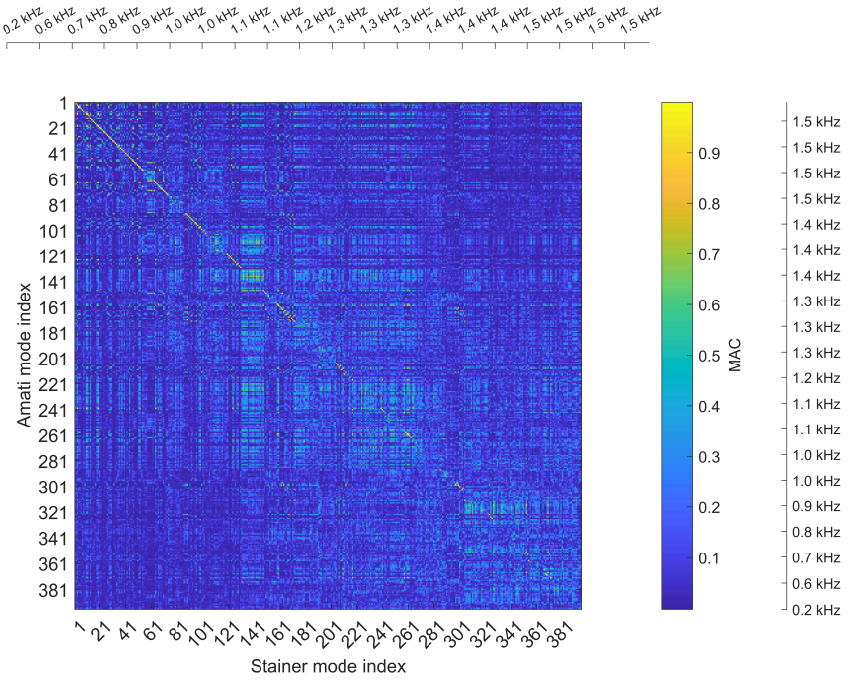

Figure 4.8: Amati-Stainer MAC Matrix

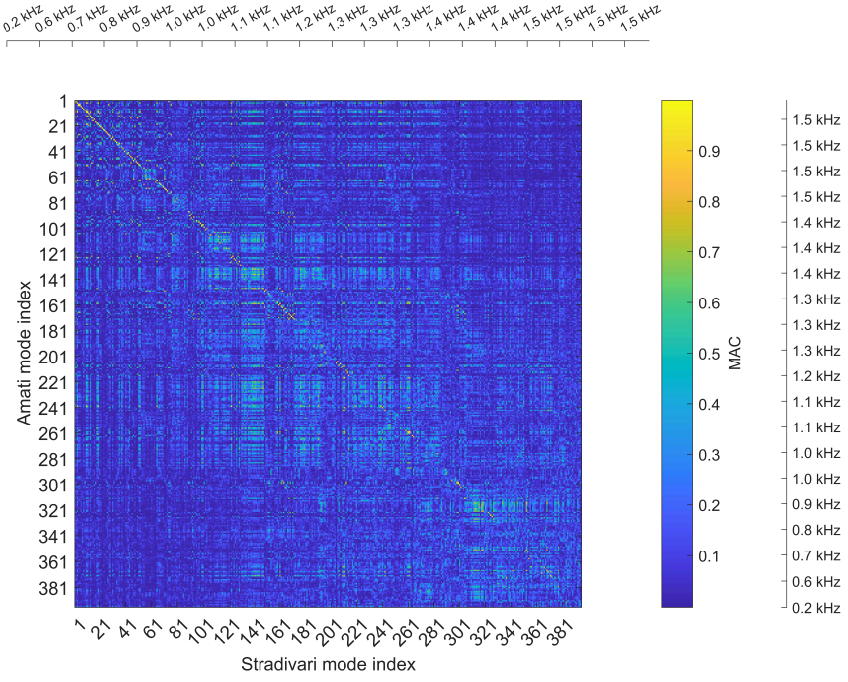

Figure 4.9: Amati-Stradivari MAC Matrix

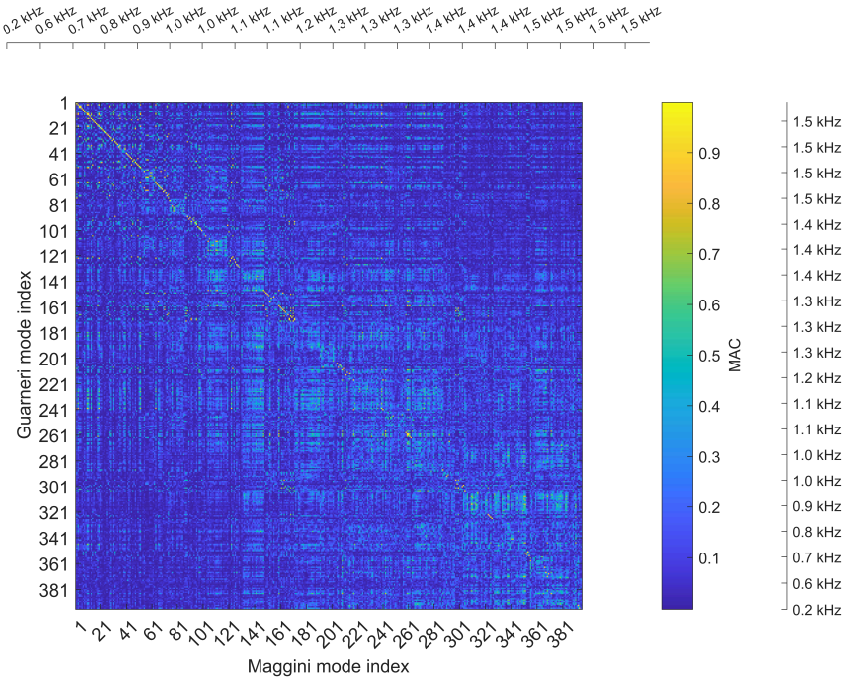

Figure 4.10: Guarnieri-Maggini MAC Matrix

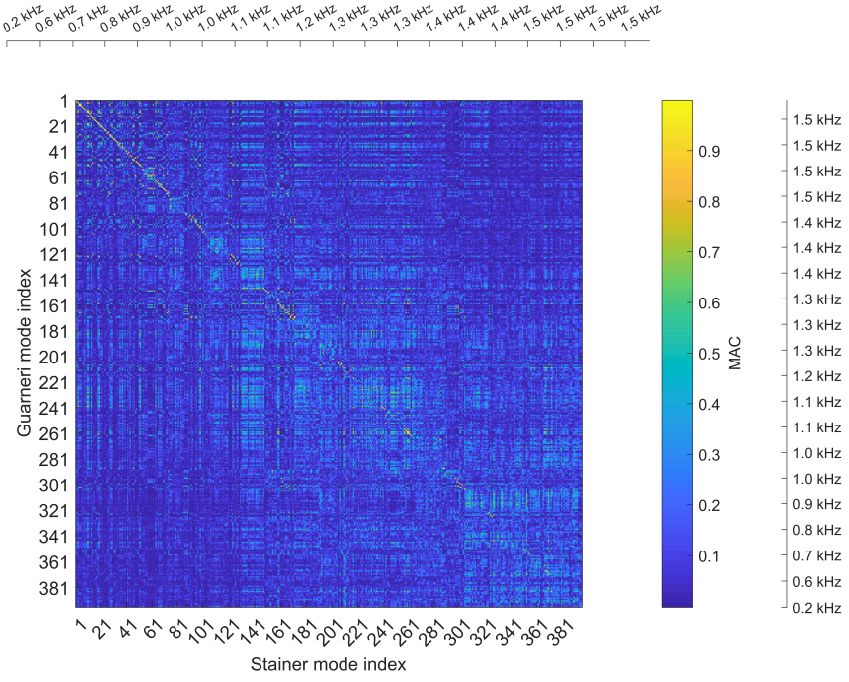

Figure 4.11: Guarnieri-Stainer MAC Matrix

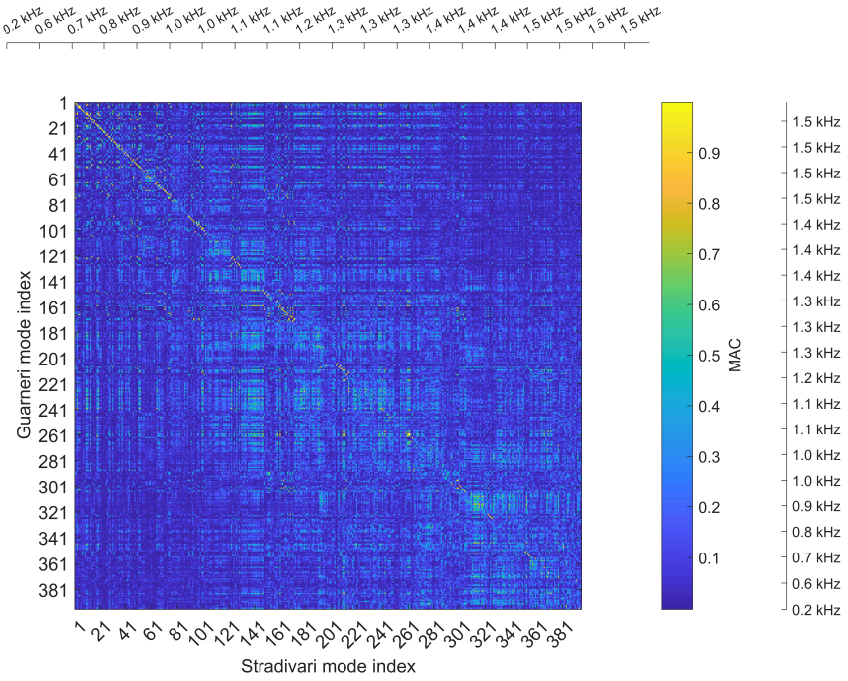

Figure 4.12: Guarnieri-Stradivari MAC Matrix

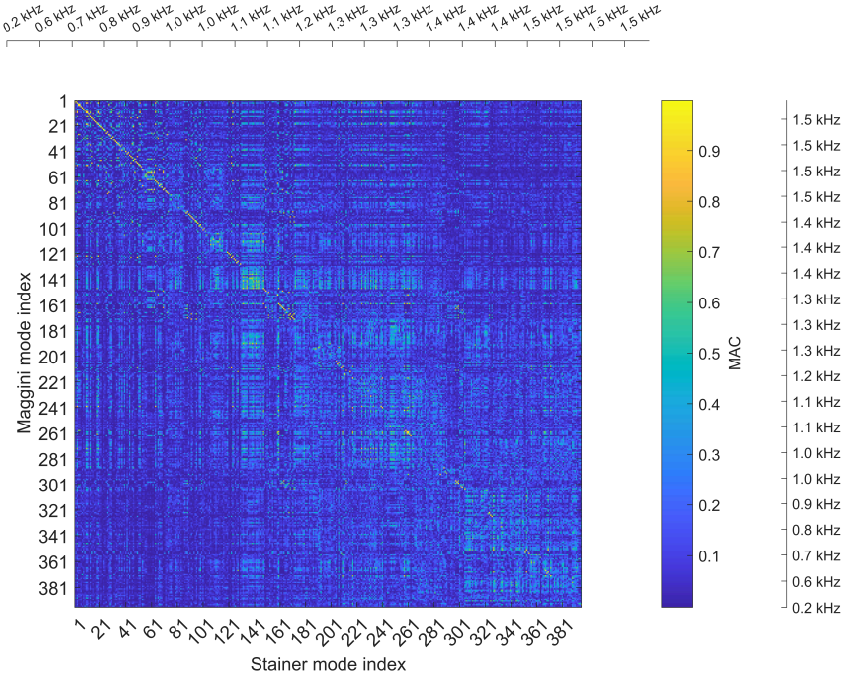

Figure 4.13: Maggini-Stainer MAC Matrix

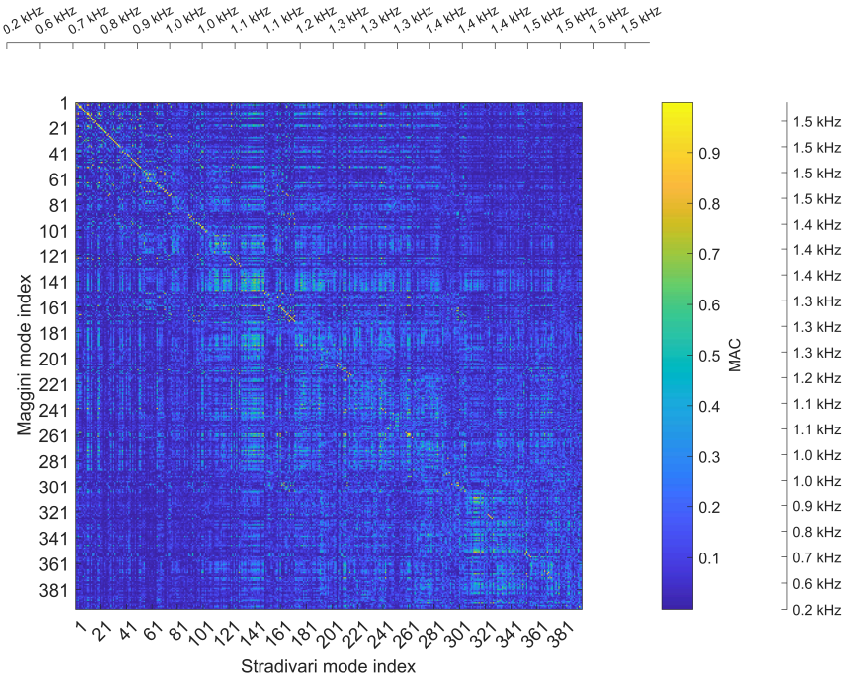

Figure 4.14: Maggini-Stradivari MAC Matrix

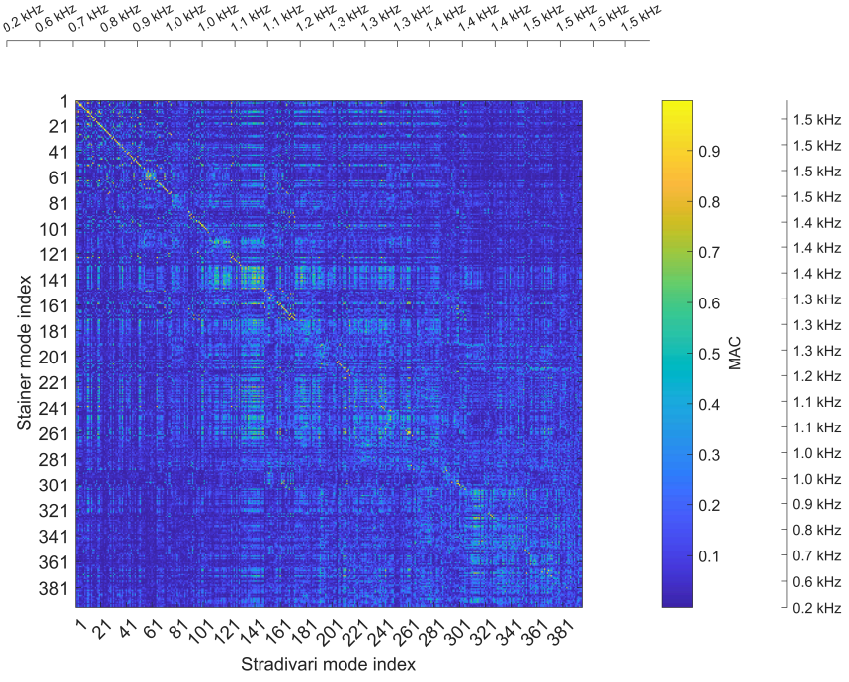

Figure 4.15: Stainer-Stradivari MAC Matrix

In these plots, the qualitative and quantitative observation of the main diagonal is important. With the aim of verifying a generic presence of mode switching, the MAC values on the main diagonal were calculated for each calculated matrix obtaining the following results:

MAC Matrix	Average MAC on the diagonal
Amati-Amati	1.0000
Amati-Guarnieri	0.3339
Amati-Maggini	0.3914
Amati-Stainer	0.4275
Amati-Stradivari	0.3225
Guarnieri-Guarnieri	1.0000
Guarnieri-Maggini	0.3639
Guarnieri-Stainer	0.3577
Guarnieri-Stradivari	0.3317
Maggini-Maggini	1.0000
Maggini-Stainer	0.3862
Maggini-Stradivari	0.3477
Stainer-Stainer	1.0000
Stainer-Stradivari	0.3444
Stradivari-Stradivari	1.0000

Table 4.3: Average value of the MAC on the main diagonal for each comparison matrix

This first quantitative analysis shows that Matrix self-MACs present mean unit values on the main diagonal confirming the consistency of the modal data. The comparison matrices between different models, on the other hand, present average values that are very far from unity, underlining that the 1:1 relationship between the vibration modes of the models is weak. Due to mode switching, frequency-close modes exchange order between different configurations, making diagonal analysis alone a little weak. To enrich the quantitative analysis, in addition to the mean value of the diagonal, several statistical indicators were calculated:

- Average value of line maxima
- Median and standard deviation of diagonal elements

The average value of the row maxima monitors the maximum correlation that each mode of a model achieves with any mode of a second model. This index is less sensitive to the

alignment of mode indices and takes into account the best possible correlation. Regarding the diagonal, in addition to the mean, median and standard deviation are calculated; the first allows us to underline the general correlation of the group of modes of one model with those of another, the second instead indicates the dispersion of MAC values along the main diagonal by detecting the variation in correlation between modes. The median is an index that is not very sensitive to small geometric differences which instead significantly alter the mean. A high value of this index suggests that most modes maintain a high overall correlation. Speaking of the standard deviation index, high values indicate a strong dispersion and therefore an irregularity in the modal correspondence.

Model pair	Mean Diagonal	Mean Row Max	Median Diagonal	Std. Diagonal
Amati vs Amati	1.0000	1.0000	1.0000	0.0000
Amati vs Guarneri	0.3339	0.6953	0.1989	0.3492
Amati vs Maggini	0.3914	0.6995	0.2400	0.3612
Amati vs Stainer	0.4275	0.7142	0.2911	0.3801
Amati vs Stradivari	0.3225	0.6913	0.2058	0.3315
Guarnieri vs Guarnieri	1.0000	1.0000	1.0000	0.0000
Guarnieri vs Maggini	0.3639	0.7021	0.2173	0.3528
Guarnieri vs Stainer	0.3577	0.6881	0.2211	0.3485
Guarnieri vs Stradivari	0.3317	0.6960	0.2098	0.3326
Maggini vs Maggini	1.0000	1.0000	1.0000	0.0000
Maggini vs Stainer	0.3862	0.7066	0.2328	0.3589
Maggini vs Stradivari	0.3477	0.6994	0.2031	0.3464
Stainer vs Stainer	1.0000	1.0000	1.0000	0.0000
Stainer vs Stradivari	0.3444	0.7005	0.2204	0.3400
Stradivari vs Stradivari	1.0000	1.0000	1.0000	0.0000

Table 4.4: Synthetic metrics from the MAC matrix

Regarding the modal extraction system, all correlation analyses through Self-MAC Matrix present unit diagonal mean and zero diagonal standard deviation, confirming its correct functioning. By analyzing the MAC matrix comparison between different models, the diagonal average values cover the range 0.3225-0.4275, marking a moderate modal correlation between modes in the same order. The average value of the line maxima, which

instead covers the range 0.6881-0.7142, is higher than the diagonal average, highlighting that, despite a moderate correspondence between modes with the same index, there are similar modes for dynamic behavior even if not perfectly aligned. This confirms that we are in the presence of a mode switching phenomenon. The median takes values between 0.1989 and 0.2911, the standard deviation between 0.3315 and 0.3612. These values indicate that the modal correlation is not uniform for all modes and that it is generally a medium-low correlation.

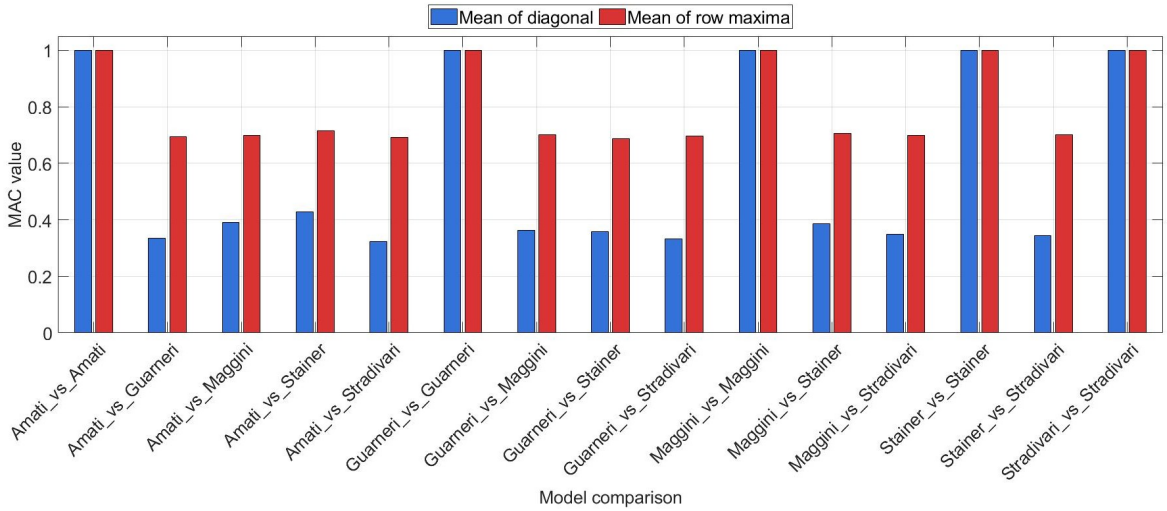

Figure 4.16: Mean diagonal vs. Mean Row Max

In summary, each of these indices contributes to making the mode switching phenomenon quantitative evidence. To conclude this, it is evident that an analysis based simply on the ordered comparison of the modalities with respect to their index cannot be conducted, but that it is necessary to consider other similarity metrics such as those used in this study.

4.4. Statistical analysis of modal and acoustic variability

The objective of this analysis is to quantitatively verify the relationship between the variability of the eigenfrequencies and the variability of the acoustic response. In MATLAB, each model provides a set of eigenfrequencies $f_{i,j}$ (where i refers to the mode and j to the model), and BEM analysis provides an SPL curve $L_{p,i}(f)$ corresponding to the frequencies. Since the eigenfrequencies of the various models do not necessarily coincide with the frequencies studied in the BEM simulation, it was necessary to carry out linear

interpolation in correspondence with each modal frequency, obtaining a sound pressure value $L_{p,j}(f_{i,j})$ for each of these precise frequencies.

Fundamental statistical quantities were then defined such as:

- Mean modal frequency: $\bar{f}_i = \text{mean}(f_{i,j})$
- Standard deviation of modal frequency: $\sigma_{f_i} = \text{std}(f_{i,j})$
- Mean acoustic response at modal frequencies: $\bar{L}_i = \text{mean}\big(L_{p,j}(f_{i,j})\big)$
- Standard deviation of acoustic response: $\sigma_{L_i} = \text{std}\big(L_{p,j}(f_{i,j})\big)$

To identify the link between vibrational variability and sound variability, two correlation coefficients were calculated: the Pearson coefficient r measures the linear correlation between the standard deviation in frequency and the acoustic pressure, while the Spearman coefficient ρ measures the monotonic correlation, not necessarily linear, to verify whether the phenomenon increases or decreases jointly.

The analysis proceeds with the discrimination between high variability and low variability modes. To do this, a statistical threshold was defined for the standard deviation of the modal frequencies and for the acoustic response:

$$\sigma_{f_i} > \text{mean}(\sigma_f) + \text{std}(\sigma_f)$$

$$\sigma_{L_i} > \text{mean}(\sigma_L) + \text{std}(\sigma_L)$$

These limits allow you to classify modes and divide them into HighFreqVar and HighRadVar groups. Through a 2x2 contingency matrix, the cases of overlapping membership in both high instability groups were quantified.

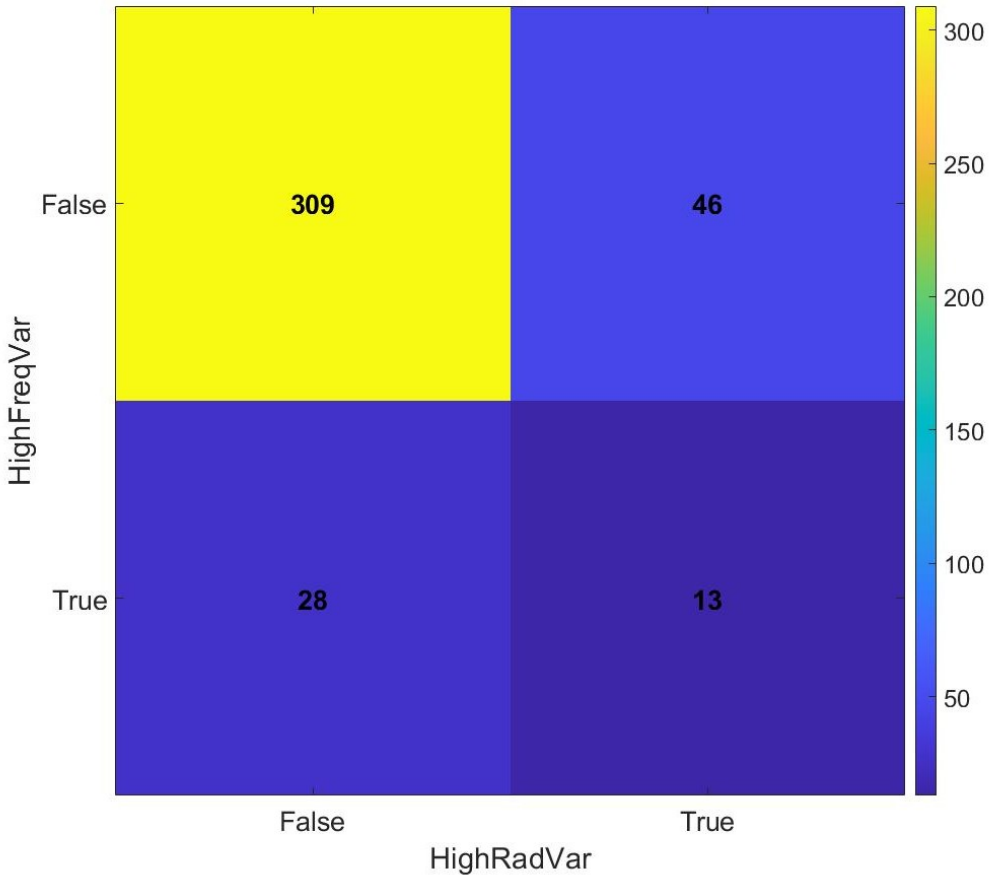

Figure 4.17: Contingency table

Two new indices were thus calculated: sensitivity and precision.

- Sensitivity: measures the probability that given a mode of high structural instability it is also so from an acoustic point of view, it is therefore a measure of propagation of instability from a mechanical domain to an acoustic domain.

$$P\big(\text{HighRad} \mid \text{HighFreq}\big)$$

- Precision: measures the probability that given a mode of high acoustic instability it is also structurally so, it is therefore a measure of randomness in the differences in acoustic response.

$$P\big(\text{HighFreq} \mid \text{HighRad}\big)$$

High sensitivity values indicate that modal instability propagates from mechanical to acoustic domains, high precision values suggest that acoustic instability is due to structural effects.

4.5. Statistical results

Modes count	n	396
Pearson coefficient r	r	0.2979
Determination coefficient	r^2	0.0887
Spearman coefficient	ρ	0.2573
Pearson p-value	p_{Pearson}	1.467×10^{-9}
Spearman p-value	p_{Spearman}	2.308×10^{-7}
Frequency threshold	th_{freq}	3.483
Acoustic threshold	th_{rad}	1.998
Sensitivity	$P(\text{HighRad} \mid \text{HighFreq})$	0.220
Precision	$P(\text{HighFreq} \mid \text{HighRad})$	0.317

Table 4.5: Statistical index results

5 | Conclusions and future developments

5.1. Summary of the study and methodology used

This thesis analyzed the influence of f-hole design on the distribution of structural stresses and acoustic radiation in the violin. The main objective was to systematically quantify how variations in the geometry of these elements simultaneously influence the instrument's mechanical and acoustic behavior. To reduce geometric complexity and isolate the impact of the f-holes, the analysis was based on a cornerless violin model. This design choice eliminates profile edges and abrupt curvature changes that can introduce unwanted local effects, allowing for a more controlled study of the role of the openings. The methodology used involves a coupled numerical simulation, combining FEM for structural analysis and BEM for acoustic analysis, which is already well established in the scientific literature for the study of musical instruments. The systematic comparison involved five historical f-hole designs by five master luthiers: Amati, Stradivari, Maggini, Guarnieri and Stainer. These designs represent significant geometric variations in relation to this scientific study, but they also represent different construction philosophies that are fundamental to the evolutionary history of f-holes. Historical models were therefore chosen to avoid arbitrary design choices in favor of geometries with already established design and historical relevance. A mathematical rather than experimental approach was chosen so that a single geometric parameter could be selectively controlled while keeping all others constant. An experimental approach would have introduced variability due to the difficulty of exactly replicating a violin, given the different characteristics that the same type of wood can take on, the thickness of the plates or the different assembly conditions. This study provides a solid methodological basis for future research, making it possible to investigate in a controlled manner how individual geometric elements influence the overall behavior of the violin.

5.2. Structural results

The structural analysis, conducted using the FEM method, revealed important details about the mechanical behavior of the soundboard in relation to the variation in the design of the f-holes. The first significant result concerns the stability of the vibration modes in the frequency range 0–1000 Hz. In this range, the geometric variation of the openings did not produce significant changes in the mode shapes, suggesting that, at lower frequencies, the overall structure of the soundboard controls the vibrational behavior rather than the local characteristics of the f-holes.

However, the introduction of openings alters the distribution of internal loads. The stress and strain analysis showed that the openings present areas of concentration of mechanical stress. The areas with the highest stress are those at the highest risk of fatigue and microfractures, i.e., those with lower structural strength, which can have a greater impact on the instrument's durability. In line with the principles of solid mechanics, these areas act as stress concentrators.

In addition to the stress distribution, it is important to understand how varying the dimensional parameters of these holes influences the overall compliance of the top plate. The study of the correlation between the geometric parameters of the f-holes and the deformation of the soundboard showed that larger perimeters and areas of the openings are generally associated with greater structural deformation, i.e., greater mechanical flexibility. Larger openings equate to greater material removal from the soundboard and consequently reduce its local stiffness, allowing for larger vibration amplitudes under the action of dynamic forces transmitted through the bridge. Linear correlation analysis between maximum deformation along the centerline of the board and the perimeter and area parameters for each type of f-hole considered showed that the deformation depends more on the perimeter of the openings than on their area. This suggests that the length of the edge of the f-holes is the most influential geometric parameter in determining the mechanical response of the soundboard, as already verified in previous studies [5].

The relationship between geometry and deformation has important design implications: f-hole designs with large perimeters and small areas tend to produce a soundboard that is more sensitive to stress. This combination may be desirable from a design perspective if the goal is to increase the violin's volume response, but the structural strength and durability of an instrument more sensitive to stresses from the bridge must also be considered. Stress and deformation analyses of the top plate have demonstrated the fundamental structural role of f-holes in shielding deformations propagating from the load-bearing area to the peripheral areas of the top plate, allowing the structure to conform to the boundary

conditions with near-zero stress. Historical luthiers have managed these tradeoffs through centuries of empirical practice, giving rise to the variety of f-hole designs present in the violin-making tradition.

5.3. Acoustic and vibration implications

The acoustic analysis, conducted using the BEM method, made it possible to quantify the impact of the geometry of the f-holes on the acoustic radiation of the violin, calculating the SPL in the far field. The results showed that variations in the design of the openings produce a quantifiable effect on the sound radiation of the violin, albeit in a non-uniform manner.

The greatest variations in SPL among the five historical designs studied are concentrated in the frequency band between 200 Hz and 2000 Hz. This region is particularly relevant from a perceptual and musical point of view, as it includes part of the violin's middle register and contributes to its characteristic timbre. The sensitivity of the SPL to geometric variations in this band demonstrates that the f-holes influence the acoustic response of the instrument, influencing both the radiated amplitude and the spectral distribution of energy. The main peak of acoustic variability, which has the maximum SPL standard deviation, was identified at 1328.4 Hz, which represents the most critical point where the geometry of the f-holes has the most pronounced effect on radiation. The identification of this critical frequency suggests that targeted modifications to the design of the openings can be used to modulate the acoustic response of the violin in specific spectral bands.

The results obtained show that the nature of the impact of geometry on SPL is not uniform. Despite the use of a simplified model, from which proportional and constant variations would be expected, the results show complex and frequency-dependent behavior, indicating that the coupling mechanisms between structural vibration and acoustic radiation are mediated by local resonance phenomena that vary significantly with frequency. The physical interpretation of these phenomena requires consideration of the dual role of the openings in the acoustic response of the instrument. In addition to allowing communication between the internal air volume and the external environment, the f-holes locally modify both the stiffness and the distribution of vibrations on the top plate, indirectly contributing to acoustic radiation. It is the combination of these two effects that produces complex acoustic behavior, in which the overall effect depends on the interaction between direct radiation due to the openings and that due to the vibrating plate.

Overall, the analysis confirms that the geometry of the openings does not simply act

as a local parameter, but influences the entire acoustic radiation of the instrument in a distributed and strongly frequency-dependent manner. However, this influence appears to be perceptually negligible, as the changes in SPL are too small to be relevant to the listener, suggesting that the design of the f-holes has little impact on the overall acoustic behavior. The results obtained therefore provide a solid and detailed quantitative basis, useful for guiding future explorations and targeted studies on the control of the vibro-acoustic response of the violin under different operating conditions.

5.4. Correlation, variability, and mode switching

The correlation analysis between vibrational and acoustic behavior highlighted complex aspects of the relationship between these two domains. To quantify the influence of geometric variability on acoustic variability and vise versa, the MAC was applied and the results were studied. This criterion allows the similarity between the modal shapes of different f-hole designs to be evaluated in order to identify any mode switching phenomena. Mode switching occurs when vibration modes that are close in frequency exchange positions as a result of changes in system parameters, which is particularly relevant in structures with symmetries [30]. The analysis of the MAC matrices confirmed the presence of this phenomenon in the comparison between the different f-hole designs. The average values on the diagonal of these comparison matrices, ranging from 0.3225 to 0.4275, indicate a moderate position correlation between modes associated with different models, suggesting that the mode associated with a given modal number of one design does not necessarily correspond to the same mode of another design. The analysis of the row maxima, whose values are higher and range between 0.6881 and 0.7142, indicates that, although there is no perfect positional correspondence between modes, there is instead a strong modal correspondence between different designs when observing the matrices in their entirety. In summary, each mode of a design finds a similar counterpart in another design, but not necessarily with the same associated modal number. This behavior is more easily observed in high modal density systems, where many modes are concentrated in narrow frequency bands with a consequent greater possibility of interchange.

5.4.1. Statistical results discussion

The statistical analysis was conducted on a dataset of 396 vibrational modes extracted from the five analyzed models to quantify the relationship between structural variability and acoustic variability. Two variability indices were calculated for each mode: structural variability, defined as the standard deviation of modal frequencies, and acoustic variability,

defined as the standard deviation of SPL.

The Pearson correlation coefficient, which measures the linear correlation between these variables, and the Spearman coefficient, which measures the monotonic correlation, were calculated. The Pearson coefficient returned a value of $r = 0.298$, while the Spearman coefficient returned a value of $\rho = 0.257$. Analyzing the coefficient values obtained, it can be stated that there is no correlation between the structural and acoustic domains, neither linear nor monotonic. The statistical results obtained demonstrate that the correlation is too weak to be considered significant in interpreting and predicting the physical behavior of the system. The correlation coefficient, which recorded a value of r^2=0.089, quantifies this lack of direct correlation. In fact, only 8.87% of the acoustic variation is explained by a corresponding variability in the structural domain, indicating that the remaining 91.13% is attributable to other factors. This demonstrates that the geometric variations of the f-holes modify the mechanical response, but do not influence the acoustic response in a linear or proportional manner. Even if the structural variability could be perfectly predicted, only 8.87% of the acoustic variability could be explained. To further explore the relationship between these two domains, an analysis based on the results of the contingency tables was then conducted. This analysis is based on the binary classification of modes into "high variability" and "low variability." To do this, two thresholds were defined: a structural variability threshold ($th_{\text{freq}} = 3.483$) and an acoustic variability threshold (th_{rad}= 1.998), which allowed the dataset to be divided. The vibration modes were then classified according to these parameters for both domains under consideration. Sensitivity and precision were then calculated. Sensitivity, defined as P(HighRad | HighFreq), represents the probability that a mode with high structural variability also exhibits high acoustic variability. A value of 0.220 was recorded, indicating that only 22% of structurally unstable modes also exhibit acoustic instability. Precision, defined as P(HighFreq | HighRad), represents the probability that a mode with high acoustic variability also exhibits high structural variability. The resulting value of 0.317 indicates that 31.7% of the acoustically unstable modes simultaneously exhibit high structural variability. The low sensitivity and precision values confirm the complex and nonlinear nature of the relationship. A mode can be structurally stable and acoustically unstable, or vice versa, indicating that radiation mechanisms depend on factors beyond modal frequency characteristics.

In summary, the statistical results highlight that the geometry of the openings influences the structural and acoustic response through complex mechanisms that cannot be described by linear or monotonic correlations between parameters. Radiation efficiency therefore depends not only on frequency, but on multiple interconnected physical factors,

necessitating the use of modeling approaches that simultaneously integrate structural, acoustic, and fluid-structure coupling aspects.

5.5. Future developments

While the quantitative mapping provided by this thesis provides a solid foundation for f-hole design, the challenge of translating this data into objective acoustic quality remains. The wide variety of linguistic terms used by musicians to describe timbre reflects a complexity that technical analysis can only partially capture. To fill this gap, future research should integrate perceptual thresholds, which define the minimal spectral variations detectable by musicians, with linguistic mapping of descriptors such as "brightness" or "darkness." The results obtained in this thesis, which analyzes the influence of the various geometric components with a holistic approach that includes the coupling between soundboard, back and cavity considering their mutual influence [18], explain only a part of the complex relationship between geometry and the instrument's vibroacoustic response. Future developments could employ inverse problems solved via neural networks [22] to obtain specific material parameters for each sample. This would allow for digital twins of real instruments, identifying how the natural variability of the wood interacts with the f-hole geometry. From a physical modeling perspective, a more rigorous approach would involve a fully coupled fluid-structure interaction (FSI). Such a model would provide a more accurate description of the effect of air loading at the f-hole edges than sequential FEM-BEM schemes. Furthermore, the introduction of a physical model of bow-string interaction would enable simulation of the violin under real-world operating conditions, facilitating direct comparison with experimental measurements [18]. Furthermore, future studies could incorporate time-hardening creep models to evaluate the long-term aging process and structural evolution of the instrument under constant string loading [54]. Future research should focus on integrating these FEM-BEM models with numerical optimization algorithms and machine learning metamodels. Building on the data-driven approach proposed in 2021 [21], which successfully applied neural networks to optimize the contour and thickness profiles of violin soundboards, future studies could extend this methodology to f-hole configurations. This would enable the automatic identification of optimal geometries tailored to specific acoustic objectives, providing luthiers with a supporting quantitative tool.

Taken together, these developments indicate that the numerical approach adopted represents a solid yet still expandable foundation for the study of the violin's vibro-acoustic system. The integration of advanced modeling, geometric optimization, and experimental

validation offers a concrete perspective for future research aimed at both the physical understanding of the phenomenon and the quantitative support for violin design.

Bibliography

[1] Claudia Fritz, Joseph Curtin, Jacques Poitevineau, Hugues Borsarello, Indiana Wollman, Fan-Chia Tao, and Thierry Ghasarossian. Soloist evaluations of six old italian and six new violins. *Proceedings of the National Academy of Sciences*, 111(20):7224–7229, 2014. doi: 10.1073/pnas.1323367111. URL `https://www.pnas.org/doi/abs/10.1073/pnas.1323367111`.

[2] Charalampos Saitis, Claudia Fritz, Gary P Scavone, Catherine Guastavino, et al. Perceptual evaluation of violins: A quantitative analysis of preference judgments by experienced players. *The Journal of the Acoustical Society of America*, 132(6): 4002–4012, 2012.

[3] Claudia Fritz and Danièle Dubois. Perceptual evaluation of musical instruments: State of the art and methodology. *Acta Acustica united with Acustica*, 101(2):369–381, 2015. doi: 10.3813/AAA.918833.

[4] Samuel D. Bellows and D. Nakayama. An investigation of the f-hole shape's influence on the modal response of the violin. *Acta Acustica*, 8:67, 2024. doi: 10.1051/aacus/2024074. URL `https://doi.org/10.1051/aacus/2024074`.

[5] H. T. Nia, A. D. Jain, Y. Liu, M. R. Alam, R. drnas, and N. C. Makris. The evolution of air resonance power efficiency in the violin and its ancestors. *Proceedings of the Royal Society A: Mathematical, Physical and Engineering Sciences*, 471(2175): 20140905, 2015. doi: 10.1098/rspa.2014.0905. URL `https://doi.org/10.1098/rspa.2014.0905`.

[6] Romain Viala, Vincent Placet, Emmanuel Foltête, and Scott Cogan. Model based ranking of the influence of geometry and materials on the dynamical behavior of the violin highlights predominance of geometrical choices. *Scientific Reports*, 14, 11 2024. doi: 10.1038/s41598-024-79497-7.

[7] UC Berkeley TAFLab. Acoustics of sound holes in musical instruments, n.d. URL `https://taflab.berkeley.edu/acoustics-of-sound-holes-in-musical-instruments/`. Accessed: 2025-11.

[8] Jose Donoso, Alberto Tannús, Francisco Guimarães, and Thiago de Freitas. The physics of the violin. *Revista Brasileira de Ensino de Física*, 30:2305.1–2305.21, 12 2007.

[9] Samuel D. Bellows and Daisuke Nakayama. Modeling and measurements of the f-hole shape's influence on the bending modes of a fractional-size violin. In *Proceedings of Forum Acusticum 2023*, pages 1193–1200. European Acoustics Association, 2023. doi: 10.61782/fa.2023.0768. URL `https://dael.euracoustics.org/confs/landing_pages/fa2023/000768.html`.

[10] Massachusetts Institute of Technology. Violin makers tweak shapes for better acoustic power, 2015. URL `https://news.mit.edu/2015/violin-acoustic-power-0210`. Accessed: 2025-11.

[11] Corilon Violins. Guarneri: Cremonese violin making in stradivari's shadow, n.d.. URL `https://www.corilon.com/gb/library/master-portraits/guarneri-cremonese-violin-making-in-stradivari-s-shadow`. Accessed: 2025-11.

[12] Smithsonian Institution. Instrument makers of the stainer family, n.d. URL `https://www.si.edu/spotlight/violins/stainer`. Accessed: 2025-11.

[13] Alvin Thomas King. How stradivari positioned the f-holes, 2004. URL `https://fiddleheadstrings.com/microsoft%20word%20-%20for%20the%20strad%20part%202%208%20sept.pdf`. Accessed: 2025-11.

[14] Archivio della Liuteria Cremonese. 1726 violino chanot-chardon-braga, n.d. URL `https://www.archiviodellaliuteriacremonese.it/en/strumenti/1726_violino_chanot_chardon_braga.aspx?f=457975`. Accessed: 2025-11.

[15] Corilon Violins. Chanot: sulla famiglia di liutai della scuola francese, n.d.. URL `https://www.corilon.com/it/biblioteca/ritratti-del-maestri/chanot-famiglia-di-liutai-della-scuola-francese`. Accessed: 2025-11.

[16] Colin Gough. Violin plate modes. *Journal of the Acoustical Society of America*, 137(1):139–153, 2015. URL `https://violinacoustics.com/wp-content/uploads/2015/08/violin-plate-modes-jasa-1371-139-153-2015.pdf`. Accessed: 2025-11.

[17] E. Kaselouris, M. Bakarezos, M. Tatarakis, N. A. Papadogiannis, and V. Dimitriou. A review of finite element studies in string musical instruments. *Acoustics*, 4(1): 183–202, 2022. doi: 10.3390/acoustics4010012.

[18] Jim Woodhouse. The acoustics of the violin: a review. *Reports on Progress in Physics*, 65(4):483–524, 2014. doi: 10.1088/0034-4885/65/4/202. URL `https://iopscience.iop.org/article/10.1088/0034-4885/65/4/202`.

[19] Zai-You Yan. Simulation of sound structure interactions by the coupled fem/bem. *Int. J. Comp. Meth. and Exp. Meas.*, 6(6):1067–1078, 2018. Accessed: 2025-11.

[20] Marold Moosrainer and Helmut Fleischer. *Application of BEM and FEM to musical instruments*, pages 377 – 409. WIT Press, 06 2000. ISBN 1853125563, 9781853125560.

[21] Sebastian Gonzalez, Davide Salvi, Daniel Baeza, Fabio Antonacci, and Augusto Sarti. A data-driven approach to violin making. *Scientific Reports*, 11(1):9455, 2021.

[22] David Badiane, Sebastian Gonzalez, Raffaele Malvermi, Fabio Antonacci, and Augusto Sarti. A neural network-based method for spruce tonewood characterization. *The Journal of the Acoustical Society of America*, 154:730–738, 08 2023. doi: 10.1121/10.0020559.

[23] G. Longo, S. Gonzalez, F. Antonacci, and A. Sarti. Predicting the acoustics of archtop guitars using an ai-based algorithm trained on fem simulations. In *Proceedings of Forum Acusticum 2023*. European Acoustics Association, 2023. doi: 10.61782/fa.2023.0662.

[24] Neville H. Fletcher and Thomas D. Rossing. *The Physics of Musical Instruments*. Springer-Verlag, New York, 2nd edition, 1998.

[25] George Bissinger. Violin f-hole contribution to far-field radiation via patch near-field acoustical holography. *The Journal of the Acoustical Society of America*, 121(6):3899–3906, 2007.

[26] Henna Tahvanainen, Sebastian Gonzalez, Riccardo Bella, and Fabio Antonacci. On the role of air in string instruments. 05 2024.

[27] Jesús Alejandro Torres, Carlos A. Soto, and David Torres-Torres. Exploring design variations of the titian stradivari violin using a finite element model. *The Journal of the Acoustical Society of America*, 148(3):1496–1506, 2020. doi: 10.1121/10.0001952.

[28] M. Lercari, S. Gonzalez, C. Espinoza, G. Longo, F. Antonacci, and A. Sarti. Using mechanical metamaterials in guitar top plates: A numerical study. *Applied Sciences*, 12(17):8619, 2022. doi: 10.3390/app12178619.

[29] Simone Fernando Sacconi. *I "segreti" di Stradivari*. Libreria del Convegno, Cremona, 1972.

[30] Elisabetta Manconi and Brian Mace. Veering and strong coupling effects in structural dynamics. *Journal of Vibration and Acoustics*, 139(2):021009, 2017. doi: 10.1115/1.4035109.

[31] Sebastian Gonzalez, Davide Salvi, Fabio Antonacci, and Augusto Sarti. Eigenfrequency optimisation of free violin plates). *The Journal of the Acoustical Society of America*, 149(3):1400–1410, 03 2021. ISSN 0001-4966. doi: 10.1121/10.0003599. URL `https://doi.org/10.1121/10.0003599`.

[32] Musikinstrumenten-Museum der Universität Leipzig. Violine (cornerless violin) by thomas hulme, manchester (1792). inventory no. 911, 1792. URL `https://mimo-international.com/MIMO/doc/IFD/OAI_ULEI_M0006062`. Accessed: 2026-01.

[33] D. Salvi, S. Gonzalez, F. Antonacci, and A. Sarti. Modal analysis of free archtop guitar top plates. *The Journal of the Acoustical Society of America*, 150(2):1505, August 2021. doi: 10.1121/10.0005937. PMID: 34470294.

[34] Voichita Bucur. *Acoustics of Wood*. Springer-Verlag, Berlin, 2nd edition, 2006. ISBN 978-3-540-26123-0. doi: 10.1007/3-540-30594-7.

[35] Berend C. Stoel and Terry M. Borman. A comparison of wood density between classical Cremonese and modern violins. *PLOS ONE*, 3(7):e2554, 2008. doi: 10.1371/journal.pone.0002554.

[36] Masao Yokoyama, Riccardo Roberto De Lucia, Fabio Antonacci, and Augusto Sarti. Influence of orthotropic properties on vibration of violin top plates. In *Proceedings of the 23rd International Congress on Acoustics (ICA 2019)*, pages 5564–5570, Aachen, Germany, 2019. doi: 10.18154/RWTH-2019-09383.

[37] George A. Knott. A modal analysis of the violin using MSC/NASTRAN and PATRAN. *Finite Elements in Analysis and Design*, 3(4):269–280, 1987. doi: 10.1016/0167-8973(87)90014-4.

[38] A. Isaksson, H. O. Saldner, and N.-E. Molin. Influence of enclosed air on vibration modes of a shell structure. *Journal of Sound and Vibration*, 187(3):451–466, 1995. doi: 10.1006/jsvi.1995.0536.

[39] Andrzej Kabała, Benedykt K. Niewczyk, and Bartosz Gapiński. Violin bridge vibrations – fem. *Vibrations in Physical Systems*, 29:2018021–1–2018021–7, 2018. URL `https://api.semanticscholar.org/CorpusID:155802018`.

[40] Juan A. Torres and Ricardo R. Boullosa. Influence of the bridge on the vibrations

of the top plate of a classical guitar. *Applied Acoustics*, 70(11-12):1371–1377, 2009. doi: 10.1016/j.apacoust.2009.07.002.

[41] John C. Schelleng. The violin as a circuit. *The Journal of the Acoustical Society of America*, 35(3):326–338, 1963. doi: 10.1121/1.1918462.

[42] Frederick A. Saunders. Recent work on violins. *The Journal of the Acoustical Society of America*, 25(3):491–498, 1953.

[43] Rodney Jones. The f-holes and the violin. *The Strad*, 108(1284):391–395, 1997. Reprinted in Journal of the Catgut Acoustical Society.

[44] Joe Wolfe. Violin acoustics: an introduction. Music Acoustics Group, University of New South Wales, 2005. URL `https://newt.phys.unsw.edu.au/jw/violin.html`. Accessed: 2026-01.

[45] Joe Wolfe. What are f-holes for? University of New South Wales, Music Acoustics, 2004. URL `https://phys.unsw.edu.au/music/people/fholes.pdf`. Accessed: 2026-01.

[46] Forest Products Laboratory. Wood handbook, chapter 5: Mechanical properties of wood, 2010. URL `https://studylib.net/doc/27976196/chapter-05`. Accessed: 2026-01.

[47] A. Bermúdez, P. Gamallo, L. M. Hervella-Nieto, R. Rodríguez, and D. Santamarina. Fluid-structure acoustic interaction. In *Advances in Mathematical and Computational Methods in Engineering*. CIMNE, Barcelona, Spain, 2005. URL `http://numat.usc.es/pub/FluidStructureAcousticInteraction.pdf`.

[48] Leilei Chen, Wenchang Zhao, Cheng Liu, and Haibo Chen. 2d structural acoustic analysis using the fem/fmbem with different coupled element types. *Archives of Acoustics*, 42(1):37–48, 2017. doi: 10.1515/aoa-2017-0005. URL `https://doi.org/10.1515/aoa-2017-0005`.

[49] Masaaki Yokoyama. Coupled numerical simulations of the structure and acoustics of a violin body. *The Journal of the Acoustical Society of America*, 150(3):2058–2064, 2021. doi: 10.1121/10.0006208.

[50] International Organization for Standardization. *ISO 3745:2012. Acoustics – Determination of sound power levels and sound energy levels of noise sources using sound pressure – Precision methods for anechoic rooms and hemi-anechoic rooms*. ISO, Geneva, Switzerland, 2012. Accessed: 2026-01.

[51] Gabriel Weinreich, Colin Holmes, and Maureen Mellody. Air-wood coupling and the swiss-cheese violin. *The Journal of the Acoustical Society of America*, 108(5): 2389–2402, 2000. doi: 10.1121/1.1314397.

[52] E. Jansson. *Acoustics for Violin and Guitar Makers*. Kungl Tekniska Hogskolan, 2002. URL `https://books.google.it/books?id=_QlTwAEACAAJ`.

[53] H. Behnke. A numerically rigorous proof of curve veering in an eigenvalue problem for differential equations. *Zeitschrift für Analysis und ihre Anwendungen*, 15(1):181–200, 1996. ISSN 0232-2064.

[54] E. Tunlid and J. Värelä. Experimental characterization and computational dynamic modelling of a violin: An analysis of the effects of creep and string tension. Master's thesis, Lund University, Department of Construction Sciences, Lund, Sweden, 2020.

List of Figures

List of Tables

List of Symbols

Variable	Description	SI unit
t	Time	s
A	Area	m^2
V	Volume	m^3
c	Speed of sound	m/s
p	Acoustic pressure	Pa
ω	Angular frequency	rad/s
ρ	Material density	kg/m^3
u	Displacement field	m
σ	Cauchy stress tensor	Pa (or N/m^2)
E	Young's Modulus (E_L, E_R, E_T)	Pa
G	Shear Modulus (G_{LR}, G_{RT}, G_{LT})	Pa
ν	Poisson's ratio ($\nu_{LR}, \nu_{RT}, \nu_{LT}$)	Dim.less
K	Stiffness Matrix (FEM)	-
M	Mass Matrix (FEM)	-
λ	Eigenvalue, $\lambda = \omega^2$	s^{-2}
f_i	Natural frequencies	Hz
C	Stiffness Tensor for orthotropic elasticity	Pa (or N/m^2)
ε	Strain Tensor	Dim.less
u_z	Vertical displacement component	m
SPL	Sound Pressure Level	dB
MAC	Modal Assurance Criterion	Dim.less
ϕ	Eigenvector (modal shape)	m